Data analysis. All values are expressed as means ± SD. Differences between groups were compared by one-way ANOVA and Bonferroni's post hoc test. Two-group analysis was performed with a Student's *t*-test. The level of significance was set at $P < 0.05$.

RESULTS

Expression of TRPA1 mRNA in human cardiac fibroblasts. We investigated the expression of TRPA1 in human cardiac fibroblasts (Fig. 1*A*). TRPA1 mRNA was detected in human cardiac fibroblasts. The amplitude of cDNA fragments was of predicted molecular size (317 bp), identical to cDNA fragments amplified from reversely transcripted mRNA.

The expression level of TRPA1 and TRP family mRNA members (TRPC1, TRPM2, TRPV1, and TRPV2) was compared by real-time quantitative RT-PCR analysis (Fig. 1*B*). Transcript levels were normalized to 18S ribosomal housekeeping gene. Significant expression of TRPA1, TRPC1, TRPV1, and TRPV2 mRNA was observed. The relative abundance of TRP mRNA was TRPA1>TRPV2>TRPC1>TRPV1. Thus TRPA1 appears to be dominantly expressed in human cardiac fibroblasts.

Expression of TRPA1 protein in human cardiac fibroblasts (immunocytochemistry and Western blotting). To confirm TRPA1 protein expression, Western blot analysis was performed. A specific antibody for TRPA1 channel protein revealed a strong band as shown in Fig. 1*C*. Expression of TRPA1 was also confirmed by immunocytochemistry in human cardiac fibroblasts as shown in Fig. 1*D*. The cells were also counterstained with DAPI to visualize nuclei, and double staining of nucleus and TRPA1 channel protein. No significant expression was detected in negative controls with normal rabbit IgG instead of a primary antibody (Fig. 1*D*, right part). These Western blotting and immunocytochemical analysis showed the expression of TRPA1 in human cardiac fibroblasts.

It has been reported that high glucose modulates the expression of TRPC such as TRPC6 (29, 73). Therefore, we investigated the effects of high glucose (20 and 30 mM) on TRPA1 expression. As shown in Fig. 1*E*, treatment of human cardiac fibroblasts with high glucose (20 and 30 mM) for 24 and 48 h did not significantly affect the expression of TRPA1 protein, compared with the control solution (5.4 mM glucose).

Effects of MG and AITC on $[Ca^{2+}]_i$ in human cardiac fibroblasts. The above results suggest that the definite expression of TRPA1 was observed in human cardiac fibroblasts. Therefore, to investigate whether TRPA1 can function in cardiac fibroblasts, the $[Ca^{2+}]_i$ measurement using fura-2 AM was applied. The effects of a dicarbonyl compound MG, an agent to activate TRPA1 (13, 26, 53), which is produced during glucose metabolism and in higher levels under hyperglycemic conditions, on $[Ca^{2+}]_i$ were investigated. In the presence of extracellular Ca^{2+}, MG (500 μM) significantly induced an increase of $[Ca^{2+}]_i$ (Fig. 2*A*). In contrast, in a cell bathed into the Ca^{2+}-free standard solution, MG (500 μM; Fig. 2*B*) did not significantly increase $[Ca^{2+}]_i$. These results suggest that MG mainly increased $[Ca^{2+}]_i$ due to Ca^{2+} entry, but not Ca^{2+} release from intracellular store sites in human cardiac fibroblasts.

Figure 3 shows the concentration-dependent effects of MG (10–1,000 μM) on $[Ca^{2+}]_i$. MG significantly increased $[Ca^{2+}]_i$ in a concentration-dependent manner. The application of MG

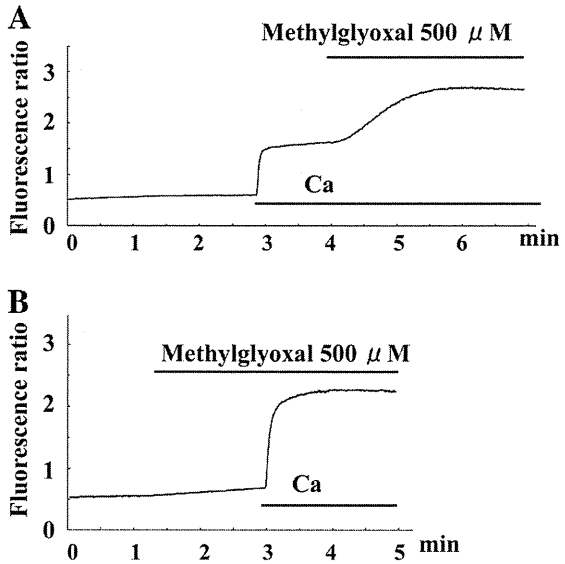

Fig. 2. Effects of methylglyoxal on intracellular Ca^{2+} concentration $[Ca^{2+}]_i$ in human cardiac fibroblasts. The Ca^{2+}-free bathing solution contained 0.9 mM EGTA in the absence of Ca^{2+}. *A* and *B*: effects of methylglyoxal (500 μM) on $[Ca^{2+}]_i$. In the presence of extracellular Ca^{2+}, methyglyoxal (*A*) increased $[Ca^{2+}]_i$. However, methylglyoxal (*B*) did not significantly increased $[Ca^{2+}]_i$ in the Ca^{2+}-free bathing solution, but the additional application of extracellular Ca^{2+} (5 mM) induced an increase of $[Ca^{2+}]_i$.

at concentrations lower than 300 μM gradually increased $[Ca^{2+}]_i$ in a concentration-dependent manner. MG (1,000 μM) induced a biphasic increase of $[Ca^{2+}]_i$. It induced a sharp peak response of $[Ca^{2+}]_i$, followed by a gradual decrease. The decay of $[Ca^{2+}]_i$ during continuous application of MG may be due to the desensitization induced by Ca^{2+} entering the channel (3, 51, 70). Figure 3*B* showed the concentration-dependent effects of MG on $[Ca^{2+}]_i$. The increased value in F340/F380 measured at the peak level or 2 min after the application of MG with reference to F340/F380 at the resting state was plotted against each concentration of MG. These results indicate that MG increased $[Ca^{2+}]_i$ dose dependently in human cardiac fibroblasts.

Figure 4*A* shows the effects of AITC, a selective TRPA1 agonist (38), on $[Ca^{2+}]_i$ in human cardiac fibroblasts. In the presence of extracellular Ca^{2+}, AITC (100 μM) significantly increased $[Ca^{2+}]_i$. The application of AITC (100 μM) induced a biphasic increase of $[Ca^{2+}]_i$ (Fig. 4*A*). The addition of AITC rapidly increased $[Ca^{2+}]_i$, and the $[Ca^{2+}]_i$ rise gradually decreased and reached to the steady state. In contrast, in a cell bathed into the Ca^{2+}-free standard solution, AITC (100 μM) did not significantly increase $[Ca^{2+}]_i$. Similarly, PGJ_2 (Fig. 4*C*, 30 μM), an agent known as other TRPA1 agonist (20), significantly increased $[Ca^{2+}]_i$.

Figure 4*B* shows the effects of MG and AITC on $[Ca^{2+}]_i$. MG (500 μM; Fig. 4*Ba*) induced an increase in $[Ca^{2+}]_i$. The additional application of AITC (100 μM) induced a further increase of $[Ca^{2+}]_i$. On the other hand, after AITC (100 μM; Fig. 4*Bb*) increased $[Ca^{2+}]_i$, the additional application of MG (100 μM) induced a only small increase in $[Ca^{2+}]_i$, suggesting that MG and AITC activated the common Ca^{2+}-influx pathways in human cardiac fibroblasts.

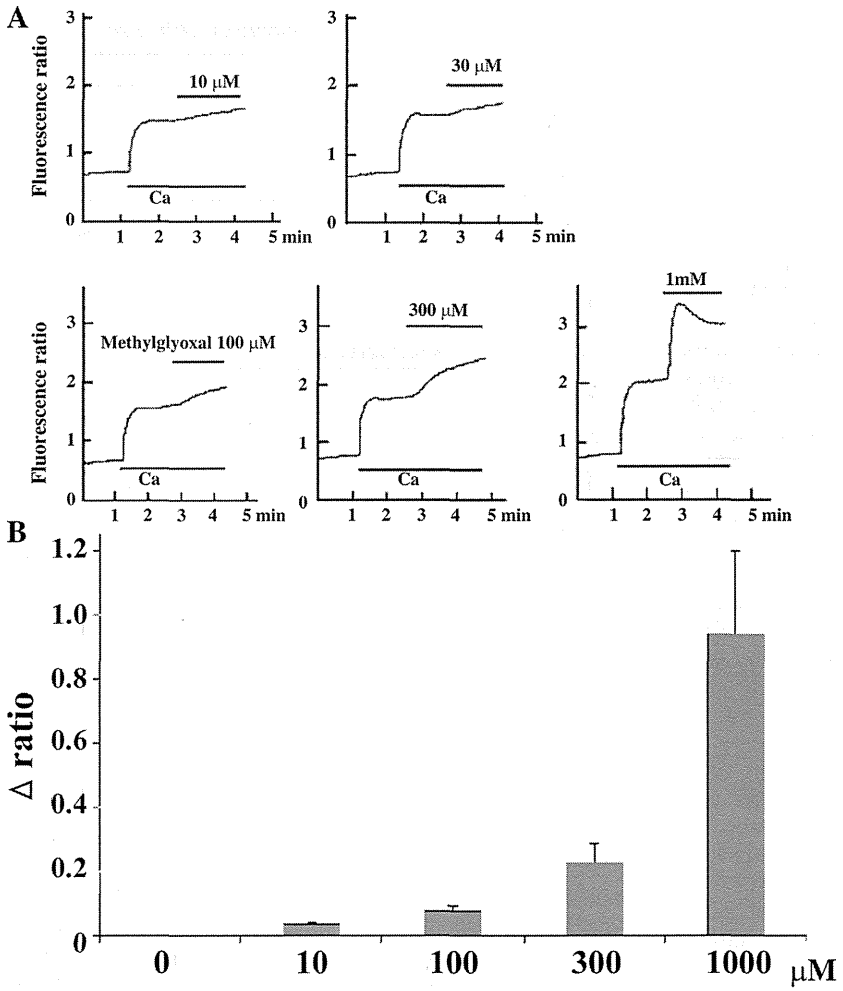

Fig. 3. Dose-dependent effects of methylglyoxal on $[Ca^{2+}]_i$. Concentration-dependent effects of methylglyoxal on $[Ca^{2+}]_I$ are shown. In *A*, the typical original traces are illustrated. The data were representative of 4 different experiments. In *B*, the increased value in F340/F380 measured 2 min after the application of methylglyoxal with reference to F340/F380 at the resting state was plotted against each concentration of methylglyoxal (0, 10, 100, 300, 1,000 μM). Each data represent the mean ± SD of paired 4 different experiments.

Effects of HC030031 and ruthenium red on MG-induced $[Ca^{2+}]_i$ increase. These results suggest the involvement of TRPA1 on MG-induced $[Ca^{2+}]_i$ increase in human cardiac fibroblasts. Therefore, we investigated the effects of HC030031 (50, 100 μM), a selective TRPA1 antagonist, on MG-induced $[Ca^{2+}]_i$ increase. As shown in Fig. 5*A*, HC030031 (100 μM) significantly inhibited the MG-induced $[Ca^{2+}]_i$ increase, compared with control cells, suggesting that TRPA1 is involved in MG-induced $[Ca^{2+}]_i$ increase in human cardiac fibroblasts. HC030031 (100 μM) inhibited MG-induced $[Ca^{2+}]_i$ rise by 71 ± 7% (n = 3; Fig. 5*B*).

Effects of various blockers on MG and AITC-induced $[Ca^{2+}]_i$. We next investigated the effects of various blockers on MG-induced $[Ca^{2+}]_i$ rise. First, we added 10 μM nicardipine, a L-type Ca^{2+} channel blocker, into the cuvette before the addition of extracellular calcium. The inclusion of 10 μM nicardipine in the bath solution did not significantly affect MG-induced Ca^{2+} entry, compared with the control cells (data not shown), suggesting that L-type Ca^{2+} channel does not significantly contribute to the Ca^{2+} influx elicited by MG in human cardiac fibroblasts. Similarly, mibefradil (10 μM), a T-type Ca^{2+} channel blocker, did not affect the $[Ca^{2+}]_i$ rise (data not shown). To further determine the type of channels involved in the calcium influx, the effects of ruthenium red (5, 10 μM), a nonselective TRP blocker including TRPA1, were investigated as shown in Fig. 5, *A* and *C*. Pretreatment with ruthenium red (10 μM; Fig. 5*A*) significantly inhibited MG-induced $[Ca^{2+}]_i$, compared with control cells. Ruthenium red (10 μM) inhibited methylglyoxal-induced $[Ca^{2+}]_i$ rise by 77 ± 11% (n = 4; Fig. 5*C*).

In addition, it is very likely that MG stimulates TRPA1 through formation of reversible hemithioacetals with cysteine residues (26). To investigate this possibility, we examined the effect of the reducing agent, DTT (10 mM), on methylglyoxal-induced $[Ca^{2+}]_i$. As shown in Fig. 5*D*, treatment of DTT (10 mM) inhibited methylglyoxal-induced $[Ca^{2+}]_i$. DTT (10 mM) inhibited MG-induced $[Ca^{2+}]_i$ rise by 81 ± 5% (n = 4; Fig. 5*E*).

Effects of aminoguanidine on MG-induced $[Ca^{2+}]_i$ rise. Figure 6 shows the effects of aminoguanidine, a MG scavenger (46, 67), on MG-induced $[Ca^{2+}]_i$ rise. The cells were pretreated with various concentrations of aminoguanidipne, and then MG was added into the bathing solution. The $[Ca^{2+}]_i$ response was compared with the control cells (untreated cells). Treatment with aminoguanidine (1–10 mM) inhibited MG-induced $[Ca^{2+}]_i$ rise in a concentration-dependent manner as shown in Fig. 6*B*.

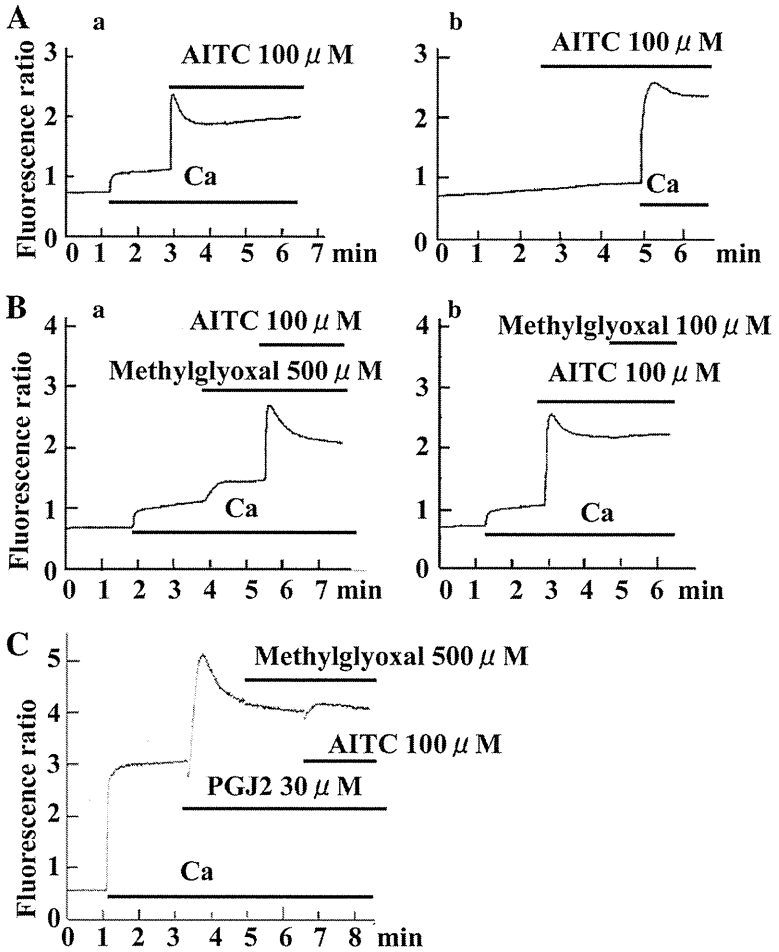

Fig. 4. Effects of methylglyoxal, allyl isothiocyanate (AITC), and PGJ_2 on intracellular Ca^{2+} concentration $[Ca^{2+}]_i$ in human cardiac fibroblasts. The Ca^{2+}-free bathing solution contained 0.9 mM EGTA in the absence of Ca^{2+}. *A*: effects of AITC on $[Ca^{2+}]_i$. In the presence of extracellular Ca^{2+}, AITC (100 μM; *Aa*) increased $[Ca^{2+}]_i$. However, AITC (100 μM; *Ab*) did not significantly increased $[Ca^{2+}]_i$ in the Ca^{2+}-free bathing solution, but the additional application of extracellular Ca^{2+} (5 mM) induced an increase of $[Ca^{2+}]_i$. *B*: effects of methylglyoxal and AITC on $[Ca^{2+}]_i$ in the presence of extracellular Ca^{2+}. Note that after AITC (100 μM; *Ab*) increased $[Ca^{2+}]_i$, the additional application of methylglyoxal induced a only small increase in $[Ca^{2+}]_i$, suggesting that methylglyoxal and AITC activated the same Ca^{2+}-influx pathways. *C*: effects of prostaglandin J2 (PGJ_2; 30 μM) on $[Ca^{2+}]_i$. After PGJ_2 (30 μM) increased $[Ca^{2+}]_i$, the additional application of methylglyoxal and AITC induced a only small increase in $[Ca^{2+}]_i$. The typical data obtained from 4 independent experiments are shown in each trace.

Effects of treatment with siRNA targeted for TRPA1 on expression level of TRPA1 mRNA and MG-induced $[Ca^{2+}]_i$ increase. To determine whether TRPA1 is involved in $[Ca^{2+}]_i$ mobilization induced by MG in human cardiac fibroblasts, we investigated the effects of siRNA targeted for TRPA1. After siRNA transfection, the level of TRPA1 mRNA expression was analyzed by real-time quantitative RT-PCR. The expression level of TRPA1 mRNA in cells transfected with siRNA significantly decreased, compared with nonsilencing (negative control) siRNA-treated cells (Fig. 7*A*). In addition, the MG-induced $[Ca^{2+}]_i$ response was compared in between siRNA- and nonsilencing (negative control) siRNA-treated cells. MG-induced $[Ca^{2+}]_i$ rise was significantly inhibited in cells transfected with siRNA for TRPA1 (Fig. 7, *B* and *C*), compared with nonsilencing (negative control) siRNA-treated cells. These results suggest that TRPA1 is mainly involved in MG-induced calcium entry from extracellular medium in human cardiac fibroblasts.

Effects of MG on cell cycle progression in human cardiac fibroblasts. We investigated the effects of MG on cell cycle. Cells were treated in the absence or presence of MG (300 μM) for 48 h and analyzed by flow cytometry. Treatment with MG (300 μM; Fig. 8) showed a larger proportion of cells entering G2/M and a smaller proportion arrested in G0/G1, compared with control cells. These results suggest that MG induced cell proliferation with cell cycle progression to S and G2/M.

Figures 9 and 10 show the effects of ruthenium red (Fig. 9, 10 μM) and HC030031 (Fig. 10, 100 μM) on MG-induced cell cycle progression in human cardiac fibroblast. Treatment with ruthenium red (Fig. 9) and HC030031 (Fig. 10) inhibited MG-induced cell cycle entry/progression with a smaller proportion of cells entering S and G2/M and a larger proportion arrested in G0/G1.

Effects of MG on cell differentiation. After fibroblasts proliferate, they differentiate into ECM proteins -secreting myofibroblasts characterized by altered morphology and increased α-SMA expression. The effects of MG on α-SMA protein expression were investigated as shown in Fig. 11. Treatment with MG (30–300 μM) for 24 h enhanced α-SMA expression as shown in Western blotting (Fig. 11, *A* and *B*). The significant staining of α-SMA was observed in cells treated with MG for 24 h (Fig. 11*C*), compared with negative control.

Figure 12, *A* and *B*, shows the effects of ruthenium red (10 μM) and HC030031 (100 μM) on MG-enhanced α-SMA expression. Treatment with MG (300 μM) enhanced α-SMA protein expression, and ruthenium red and HC030031 significantly inhibited MG-enhanced α-SMA expression as shown in Fig. 12*B*.

MG enhances α-SMA expression by a TGF-β_1-independent mechanism. To investigate whether MG enhances α-SMA expression independently of TGF-β_1, we have performed the following experiments. First, TGF-β_1 levels were evaluated by

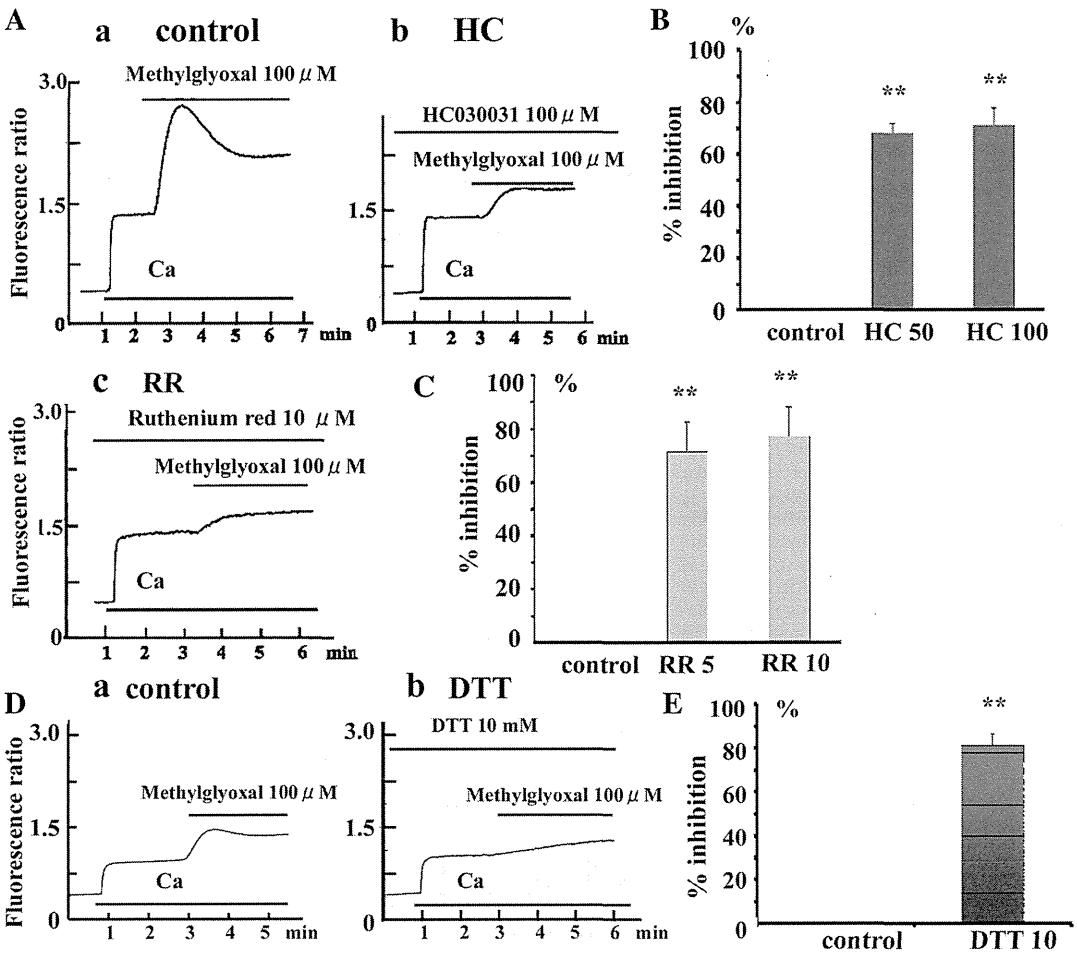

Fig. 5. Effects of HC030031, ruthenium red (RR), and DTT on methylglyoxal-induced $[Ca^{2+}]_i$ entry. Effects of HC030031 (*A* and *B*) and RR (*A* and *C*) on methylglyoxal-induced $[Ca^{2+}]_i$ rise. The cells were pretreated with these agents, and then methylglyoxal was added into the bathing solution. The $[Ca^{2+}]_i$ response was compared with the control cells (untreated cells). The typical data are illustrated in *A*. *Aa*: control cells. *Ab*: HC030031 (100 μM)-treated cells. *Ac*: RR (10 μM)-treated cells. The data were representative of 4 different experiments. *B* and *C*: inhibitory effects of HC030031 (*B*; 50 and 100 μM) and RR (*C*; 5 and 10 μM) on methylglyoxal-$[Ca^{2+}]_i$ rise. The increased value in F340/F380 induced by methylglyoxal was obtained in the absence or presence of drugs. The increased value in the absence of drugs is considered as 100%. The percent inhibition of these agents is illustrated in *B* and *C*. *D* and *E*: effects of DTT on methylglyoxal-$[Ca^{2+}]_i$ rise. The cells were pretreated with DTT for 1 min. Each datum represents the mean ± SD of paired 4 different experiments. $^{**}P < 0.01$ vs. control.

ELISA in conditioned media from MG-treated cells. Treatment of MG (300 μM) for 24 h did not significantly increase TGF-β_1 production. The concentration of TGF-β in bath solution was 34.9 ± 29.5 (in pg/ml; $n = 8$) in control, 34.1 ± 25.8 (in pg/ml; $n = 8$) in cells bathed with MG (30 μM) for 24 h, and 28.2 ± 19.9 (in pg/ml; $n = 8$) in cells bathed with MG (300 μM) for 24 h, suggesting that treatment with MG for 24 h did not enhance TGF-β_1 secretion in the present conditions. In addition, LY2157299 (0.1 and 1 μM), a potent and selective TGF-β_1 receptor blocker, did not inhibit the MG-enhanced α-SMA expression as shown in Fig. 12, *C* and *D*. These results suggest that MG enhanced α-SMA expression independently of endogenous TGF-β_1 production or activation.

DISCUSSION

The major findings of the present study are as follows. First, in human cardiac fibroblasts, MG induced Ca^{2+} entry in a concentration-dependent manner. Second, treatment with ruthenium red (RR), a general cation channel blocker, and HC030031, a selective transient receptor potential ankyrin 1 (TRPA1) antagonist, inhibited MG-induced Ca^{2+} entry. Treatment with an MG scavenger, aminoguanidine, and DTT, a reducing agent, also antagonized it. Third, AITC, a selective TRPA1 agonist, increased induced Ca^{2+} entry. The use of siRNA to knock down TRPA1 markedly reduced the MG-induced Ca^{2+} entry as well as the expression level of TRPA1 mRNA. Fourth, the conventional and quantitative real-time RT-PCR analysis showed the prominent existence of TRPA1 mRNA. Expression of TRPA1 protein was confirmed by Western blotting and immunocytochemical analyses. Finally, MG promoted cell cycle progression from G0/G1 to S/G2/M, which was significantly suppressed by treatment with HC030031 or RR. MG also enhanced α-SMA expression. The present results suggest that MG activates TRPA1 and promotes cell cycle

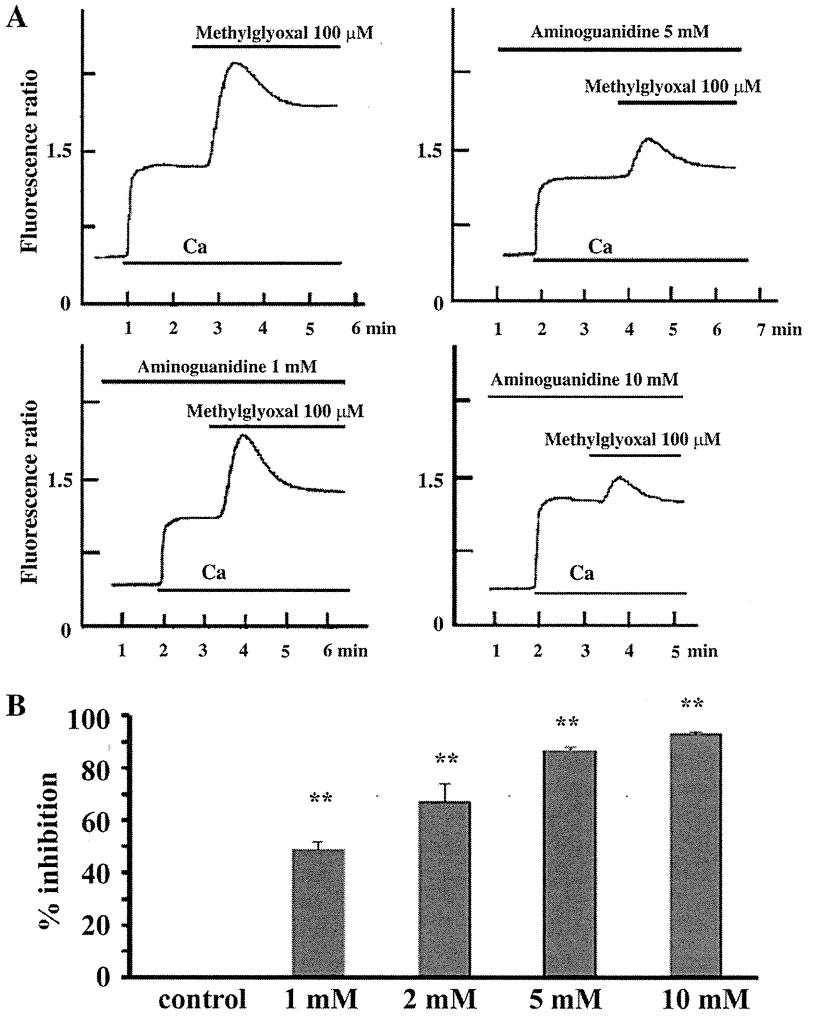

Fig. 6. Effects of aminoguanidine on methylglyoxal-induced $[Ca^{2+}]_i$ entry. *A* and *B*: effects of aminoguanidine on methylglyoxal-induced $[Ca^{2+}]_i$ rise. The cells were pretreated with various concentrations of aminoguanidipne, and then methylglyoxal was added into the bathing solution. The $[Ca^{2+}]_i$ response was compared with the control cells (untreated cells). The typical data are illustrated in *A* control cells and various concentrations of aminoguanidine-treated cells. The data were representative of 4 different experiments. *B*: effects of aminoguanidine on methylglyoxal-induced $[Ca^{2+}]_i$ rise. The increased value in F340/F380 induced by methylglyoxal was obtained in the absence or presence of drugs. The increased value in the absence of drugs is considered as 100%. The percent inhibition of these agents is illustrated in *B*. Each datum represents the mean ± SD of paired 4 different experiments. $^{**}P < 0.01$ vs. control.

progression and differentiation in human cardiac fibroblasts. MG might participate the development of pathophysiological conditions including diabetic cardiomyopathy via activation of TRPA1.

The TRP protein superfamily consists of a diverse group of cation channels in a variety of cells (47) including cardiac fibroblasts, which play an important role on physiological and pathophysiological conditions. In the present study, the expression of TRPV1, TRPV2, and TRPV4 transcripts was detected among TRPVs, and the significant expression of TRPM2, TRPM4, and TRPM7 was observed among TRPMs (data not shown). In addition, the present study provided the first evidence showing that the prominent existence of TRPA1 mRNA was observed in human cardiac fibroblasts, by using the conventional and quantitative real-time RT-PCR analysis. The expression level of mRNA was TRPA1>TRPV2>TRPC1>TRPV1. TRPA1 mRNA appears to be dominantly expressed in human cardiac fibroblasts. And, expression of TRPA1 protein was confirmed by Western blotting and immunocytochemical analyses. From these results, it is very likely that TRPA1 is functionally expressed in human cardiac fibroblasts.

TRPA1 is widely expressed in neuronal and nonneuronal cells (49), (58). The TRPA1 channel is activated by noxious cold (<17°C) and chemical compounds such as mustard oil (38). The present study provided the first evidence showing that the functional expression of TRPA1 was observed in human cardiac fibroblasts. AITC, a selective TRPA1 agonist (38), significantly increased $[Ca^{2+}]i$ in the presence of extracellular Ca^{2+}, while it failed to increase it in the absence of extracellular Ca^{2+}. MG, a dicarbonyl compound, which has been recently shown to activate TRPA1 in rat pancreatic β-cells (13), and PGJ_2, an agent known as another TRPA1 agonist (20), also significantly increased $[Ca^{2+}]i$ as well as AITC. Furthermore, after AITC increased $[Ca^{2+}]i$, the additional application of MG induced a only small increase in $[Ca^{2+}]i$, suggesting that MG and AITC activated the common Ca^{2+}-influx pathways. And, HC030031, a selective TRPA1 antagonist, and ruthenium red, a nonselective TRPA1 blocker, which can block the channel pore, inhibited MG-induced $[Ca^{2+}]i$ increase. The use of siRNA to knock down TRPA1 also markedly reduced the MG-induced Ca^{2+} entry as well as the expression level of TRPA1. Thus these results strongly suggest the involvement of TRPA1 on MG-induced $[Ca^{2+}]i$ increase in human cardiac fibroblasts. However, we have not ruled out the contribution of other ionic channels such as Ca^{2+}-activated K^+

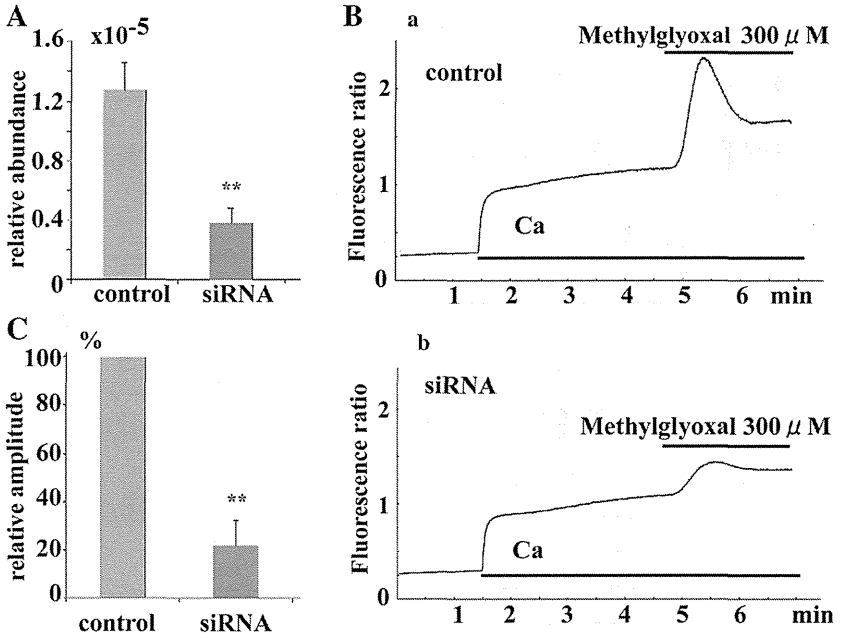

Fig. 7. Effects of treatment with small interfering RNA (siRNA) targeted for TRPA1 on expression level of TRPA1 mRNA and methylglyoxal-induced $[Ca^{2+}]_i$ increase. *A*: effects of treatment with siRNA targeted for TRPA1 on expression level of TRPA1. Human cardiac fibroblasts were treated with siRNA targeted for TRPA1 or control siRNA. Note that siRNA targeted for TRPA1 significantly decreased mRNA level of TRPA1, compared with nonsilence siRNA. $^{**}P < 0.01$ vs. control siRNA. *B* and *C*: effects of siRNA targeted for TRPA1 on methylglyoxal-induced $[Ca^{2+}]_i$ increase. The relative amplitude of methylglyoxal-induced $[Ca^{2+}]_i$ rise are plotted in nonsilence siRNA-treated and siRNA-treated cells. The increased value in nonsilence siRNA-treated cells is considered as 100%. The data were obtained from 3 different cells. $^{**}P < 0.01$ vs. control siRNA.

channels, which are functionally expressed in human cardiac fibroblasts (69), on the MG-induced Ca^{2+} moblilization as described in isolated blood vessel (50).

Long-term diabetes results in the development of diabetic cardiomyopathy. Heart failure due to diastolic ventricular dysfunction is a characteristic of diabetic cardiomyopathy and can occur during the early stages of diabetes (55). Heart cells per se are impaired in diabetic cardiomyoptahy. In addition, cardiac fibrosis is one of the pathological processes of diabetic cardiomyopathy (63) and manifests as enhanced proliferation of cardiac fibroblasts and excessive deposition of ECM, such as collagens and fibronectin. Hyperglycemia, a major pathological manifestation of diabetes, may promote the development of heart failure, primarily by causing excessive accumulation of collagen within the interstices of the myocardium, and then resulting in impaired diastolic and systolic functions (60). Intracellular Ca^{2+} has been reported to be essential for fibroblast functions. Chelating external Ca^{2+} by EGTA prevents substance P-induced proliferation of cultured rat cardiac fibroblasts (43). In human fibroblasts, it has been reported that Ca^{2+} influx is essential for the proliferation, and intracellular Ca^{2+} is required for cell cycle progression from G1/G0 to S phase (64). We have recently shown that human cardiac fibroblasts contain several TRPC-mediated Ca^{2+} influx pathways, and TGF-β_1 enhances the Ca^{2+} influx pathways requiring Ca^{2+} signals for its effect on fibroblast proliferation (35). Several papers have

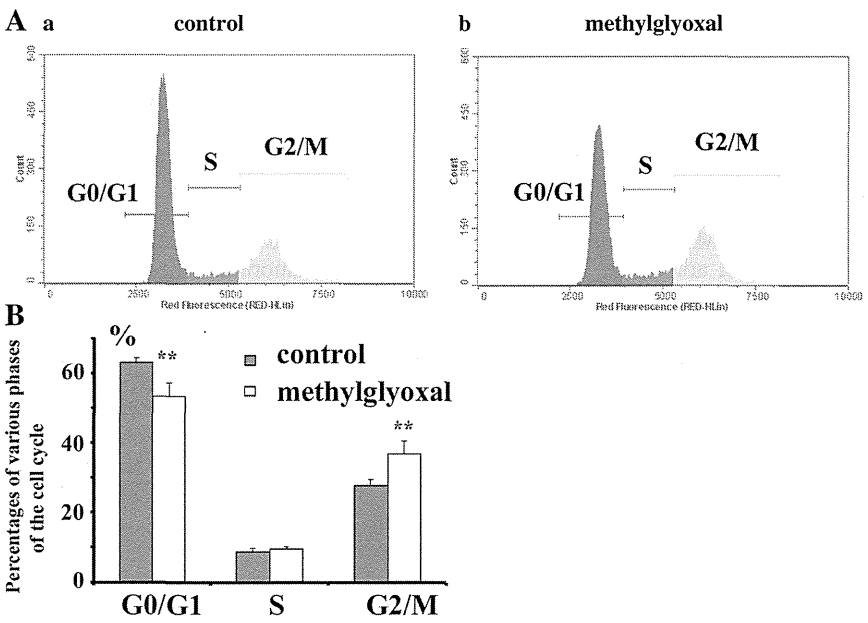

Fig. 8. Effects of methylglyoxal on cell cycle analyzed by flow cytometry. The serum-deprived cells were treated in the absence (*Aa*) or presence (*Aa*) of methylglyoxal for 48 h and analyzed by flow cytometry. Note that methylglyoxal (300 μM) induced G0/G1 to S/G2/M progression. *B*: summary data showing percentage of cells in G0/G1, S, and G2/M under control and the presence of methylglyoxal. The typical data are illustrated in this figure. The typical data obtained from 4 different experiments are illustrated in this figure. Each datum represents the means ± SD of paired 4 different experiments. $^{**}P < 0.01$ vs. control.

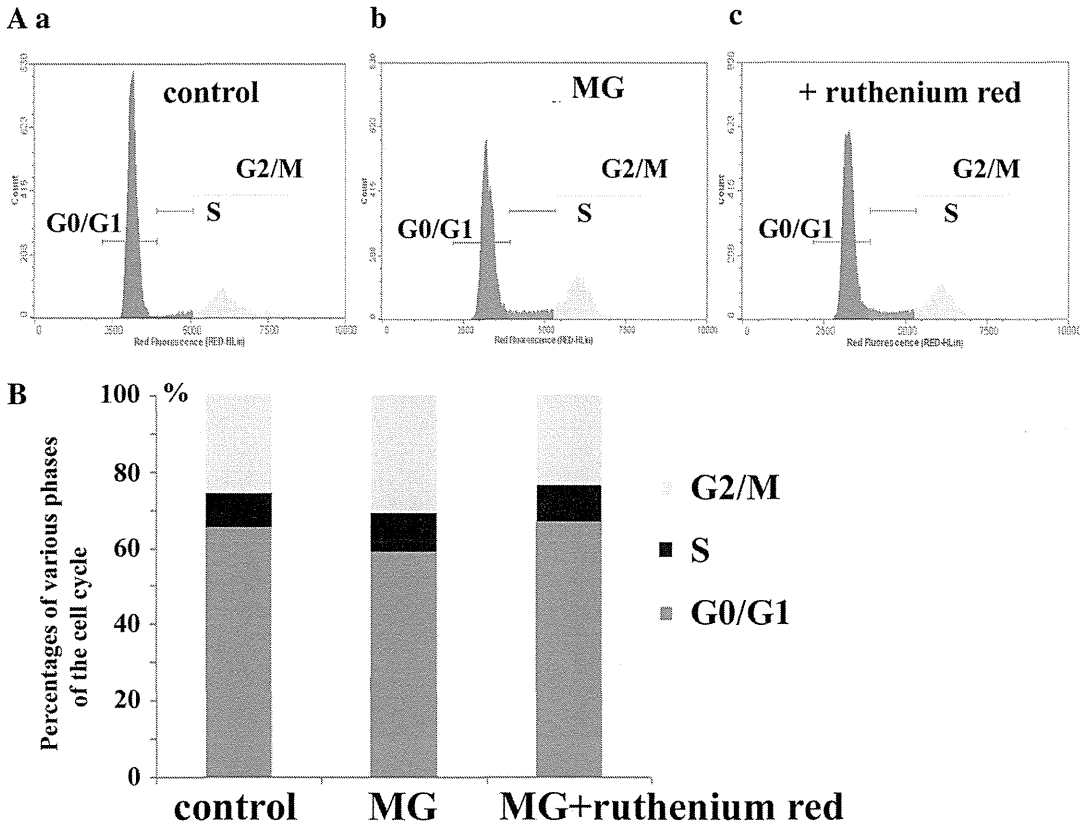

Fig. 9. Effects of ruthenium red on methylglyoxal-induced cell cycle progression analyzed by flow cytometry. The serum-deprived cells were treated in the absence (*Aa*), presence of methylglyoxal (*Ab*), and the additional application of ruthenium red (*Ac*) for 48 h and analyzed by flow cytometry. Note that methylglyoxal (*Ab*; 300 μM) induced cell cycle progression with G0/G1 to S/G2/M progression, compared with control cells (*Aa*). Treatment with ruthenium red (10 μM; *Ac*) showed a smaller proportion of cells entering S and G2/M, and a higher proportion arrested in G0/G1, compared with methylglyoxal by itself (*Ab*). *B*: summary data showing percentage of cells in G0/G1, S, and G2/M under these conditions. Groups: control, methylglyoxal, methylglyoxal plus ruthenium red.

reported that treatment of cardiac fibroblasts with high concentrations of glucose results in increased proliferation and collagen synthesis (5, 66). Dai et al. (21) also reported that high glucose induces the proliferation of cardiac fibroblasts and collagen synthesis via activation of STAT1 and STAT3. Here, we provided the first evidence showing that MG promoted cell cycle progression from G0/G1 to S/G2/M. The MG-induced cell cycle progression was significantly suppressed by treatment with HC030031, a TRPA1 specific blocker, or ruthenium red, a nonspecific TRPA1 blocker, suggesting that TRPA1 is involved in MG-induced cell cycle progression. Similarly, MG-induced cell proliferation has been described in vascular smooth muscle cells and adipocytes (14, 37). In addition, cardiac fibroblasts not only produce the ECM, but also are electrically and mechanically coupled with cardiomyocytes, resulting in affecting the electrical activity (1, 39). They cannot generate action potentials, but their membrane potential is controlled by mechanical stretch or compression of the surrounding myocardium, which in turn affects their interaction with cardiomyocytes. Thus cardiac fibroblasts appear to be dynamic participants in the physiology and pathophysiology of cardiomyocytes. Wang et al. (69) reported the contribution of BK_{Ca}-channel activity in human cardiac fibroblasts to electrical coupling of cardiomyocytes-fibroblasts. Similarly, the activation of TRPA1 induced by MG in cardiac fibroblasts may play a role in affecting electrical activity in cardiomyocytes under the pathophysiological conditions including diabetic cardiomyopathy.

Davis et al. (22) showed an obligate function for TRPC6 in promoting myofibroblast differentiation and wound healing in mice, whereas Harada et al. (32) reported the essential role of TRPC3 on rat cardiac fibroblast proliferation and differentiation. An increase in local Ca^{2+} concentration may trigger protein-protein interactions that activate downstream signaling pathways that regulate fibroblast function such as protein kinase C and ERK1/2 signaling pathway (32). The present study provided the first evidence showing the essential role of TRPA1 on MG-induced fibroblast proliferation and differentiation, but further studies are needed to clarify its downstream signaling pathways as reported in human endothelial cells (2).

After fibroblasts proliferate, they differentiate into ECM-secreting myofibroblasts characterized by altered morphology and increased α-SMA expression. The differentiation of fibroblasts into myofibroblasts is strongly upregulated in failing hearts (12), which is characterized by de novo expression of α-SMA (28). The present study also showed that α-SMA expression in human cardiac fibroblasts was enhanced by MG in a dose-dependent manner. This is compatible with the previous reports in human cardiac fibroblast used collagen gels

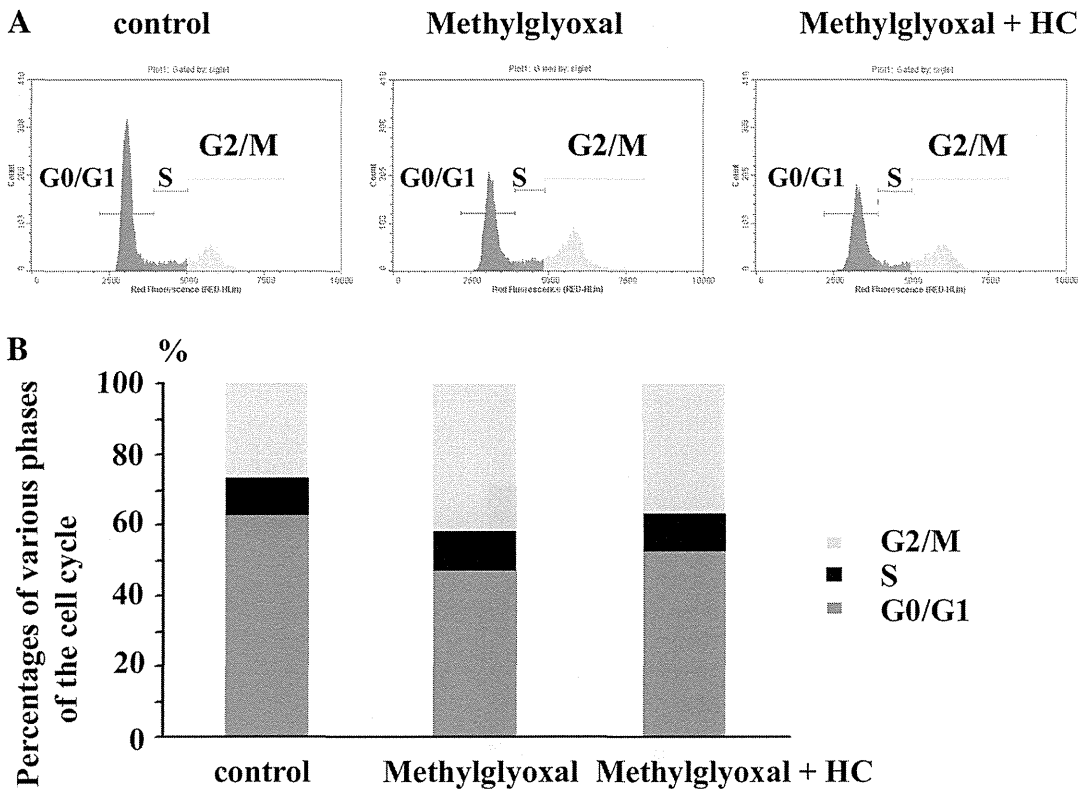

Fig. 10. Effects of HC030031 (HC) on methylglyoxal-induced cell cycle progression analyzed by flow cytometry. The serum-deprived cells were treated in the absence (*Aa*) or presence (*Ab*) of methylglyoxal, and the addition of HC030031 (100 μM) for 48 h, and analyzed by flow cytometry. Note that methylglyoxal (*Ab*; 300 μM) induced cell cycle progression with G0/G1 to S/G2/M progression, compared with control cells (*Aa*). Treatment with HC030031 (100 μM; *Ac*) showed a smaller proportion of cells entering S and G2/M, and a higher proportion arrested in G0/G1, compared with methylglyoxal by itself (*Ab*). *B*: summary data showing percentage of cells in G0/G1, S, and G2/M under these conditions. Groups: control, methylglyoxal, methylglyoxal with HC030031 (100 μM). The typical data are illustrated in this figure.

with 0.01~1 mM MG. Thus MG appears to induce human fibroblasts proliferation and enhance differentiation into myofibroblasts. Based on the results presented in this study, we propose the underlying mechanisms of MG on human cardiac fibroblasts involving the TRPA1 ion channel. Under normal conditions the TRPA1-mediated pathway may act as a low tone system to cause cell proliferation. However, in hyperglycemic conditions, production of MG can directly evoke cell proliferation and differentiation through this pathway, providing a novel signaling mechanism leading to cell proliferation. In addition, MG increased fibronectin production, an ECM (data not shown), suggesting that MG might participate the development of pathophysiological conditions including diabetic cardiomyopathy via activation of TRPA1. Further studies are needed to clarify this possibility.

Plasma levels of MG range from 1.4 to 3.3 μM in healthy humans and from 3.6 to 5.9 μM in patients with diabetes (62, 65). Therefore, MG concentrations (more than 10 μM) used in this study are high. However, it was in the range of those applied by Brouwers et al. (11) and by Cook et al. (19) to rat β-cells. Also, MG concentration of cultured Chinese hamster ovary cells has also been reported to reach up to 310 μM (15). In addition, the intracellular MG level is likely much higher than the plasma MG level in the diabetic condition because diabetic tissues are chronically (months to years) exposed to high MG levels, which may cause dramatic intracellular MG accumulation. In contrast, cultured cells were only transiently (days) exposed to high concentrations of MG, which may limit intracellular MG accumulation (16). Thus the MG concentration range (10–1,000 μM) used in the present study is not only physiologically relevant but also suitable for our in vitro experiments on cultured cells. Further work will be required to examine the longer-term effects of lower doses (~5–10 μM) of MG on the function of cardiac fibroblasts. However, the effects of MG could be antagonized by HC030031, a TRPA1 blocker, RR and he funcsiRNA traged for TRPA1, suggesting that the effects of MG are not mediated by nonspecific toxic effects, but specifically by TRPA1 channel. It has been reported that extracellular applied MG accesses specific intracellular binding sites of TRPA1 and activates it via MG-induced modification of cysteine residues (26). To investigate this possibility whether disulfide bridge formation or reversible noncovalent interactions contribute to the agonist activity of MG, the effect of the reducing agent DTT on methylglyoxal-induced $[Ca^{2+}]_i$ was investigated. DTT is expected to reduce cysteine bridges to free thiols, but also to form hemithioacetals with MG, thereby inhibiting the activation. Treatment with DTT significantly inhibited MG-induced Ca^{2+} entry, suggesting that MG may activate TRPA1 via MG-induced modification of cysteine residues. Further studies are needed to clarify the basic molecular mechanisms underlying the activation of TRPA1 caused by MG.

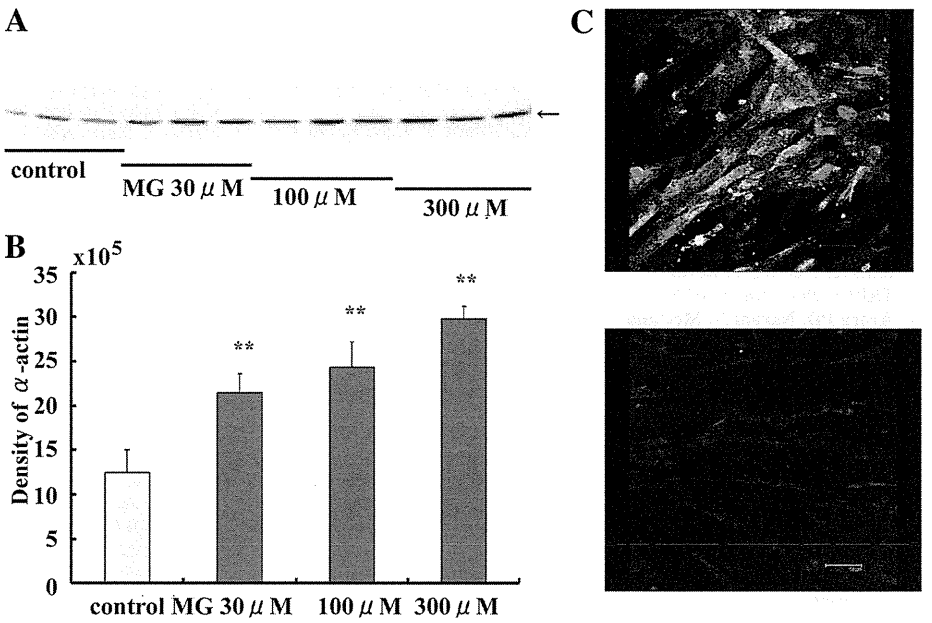

Fig. 11. Effects of methylglyoxal (MG) on α-smooth muscle actin (SMA) protein expression in human cardiac fibroblasts. *A*: effects of various concentrations of methylglyoxal on α-SMA protein expression. The cells were treated for 24 h in the absence or presence of various concentration of methylglyoxal (30–300 μM). Western blotting for α-SMA is indicated (n = 3 in each concentration). *B*: concentration-dependent effects of methyglyoxal on α-SMA protein expression analyzed by Western blotting. Each datum represents the means ± SD of the data shown in *A*. $^{**}P < 0.01$ vs. control. *C*: immunostaining for α-SMA in cells treated with methylglyoxal for 24 h. Double staining of nuclei DAPI to visualize nuclei is illustrated. Negative control is the lower part.

Limitation of the present study. We used the commercially available cultured cardiac fibroblasts obtained from healthy donors. The aspects of cardiac fibroblast phenotype, such as ion channel and receptor function and calcium modulation mechanisms, may change after isolation and during culture conditions. Therefore, further studies using intact heart are needed to clarify the usefulness and validity of conclusions from the present study.

Conclusions

The present results provide the first evidence that MG activates TRPA1 and promotes cell cycle progression and differentiation in human cardiac fibroblasts. MG might participate the development of pathophysiological conditions including diabetic cardiomyopathy via activation of TRPA1.

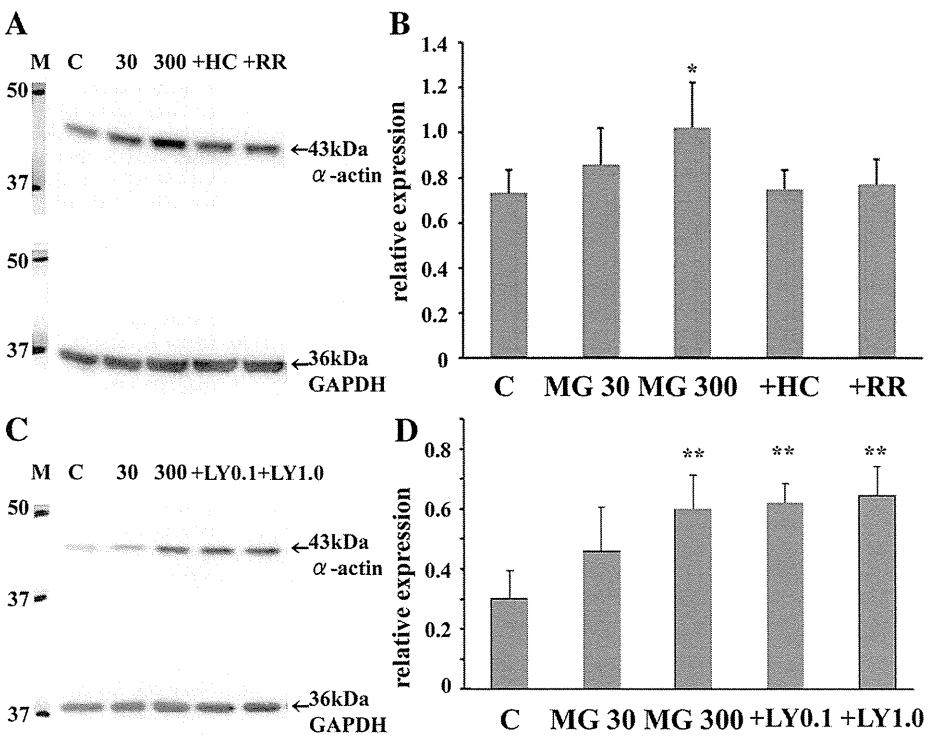

Fig. 12. Effects of ruthenium red (RR), HC030031 (HC), and LY2157299 (LY) on MG-enhanced α-SMA expression in human cardiac fibroblasts. *A* and *B*: effects of HC030031 (100 μM) and ruthenium red (10 μM) on MG-enhanced α-SMA expression analyzed by Western blotting. Treatment with ruthenium red and HC030031 significantly inhibited MG-enhanced α-SMA expression. *C* and *D*: effects of LY2157299 (0.1 and 1 μM) on MG-enhanced α-SMA expression. The α-SMA expression was measured by Western blotting, and the ratio of α-SMA 1optical density to the corresponding GAPDH optical density is shown. Each datum represents the means ± SD of paired 3 different experiments. $^{*}P < 0.05$; $^{**}P < 0.01$ vs. control. Note that LY2157299 did not inhibit the MG-enhanced α-SMA expression, as shown in *C* and *D*.

REFERENCES

1. **Abramochkin DV, Lozinsky IT, Kamkin A.** Influence of mechanical stress on fibroblast-myocyte interactions in mammalian heart. *J Mol Cell Cardiol* 70: 27–36, 2014.
2. **Akhand AA, Hossain K, Mitsui H, Kato M, Miyata T, Inagi R, Du J, Takeda K, Kawamoto Y, Suzuki H, Kurokawa K, Nakashima I.** Glyoxal and methylglyoxal trigger distinct signals for map family kinases and caspase activation in human endothelial cells. *Free Radic Biol Med* 31: 20–30, 2001.
3. **Andersson DA, Gentry C, Light E, Vastani N, Vallortigara J, Bierhaus A, Fleming T, Bevan S.** Methylglyoxal evokes pain by stimulating TRPA1. *PLoS One* 8: e77986, 2013.
4. **Arora PD, Narani N, McCulloch CA.** The compliance of collagen gels regulates transforming growth factor-beta induction of alpha-smooth muscle actin in fibroblasts. *Am J Pathol* 154: 871–882, 1999.
5. **Asbun J, Manso AM, Villarreal FJ.** Profibrotic influence of high glucose concentration on cardiac fibroblast functions: effects of losartan and vitamin E. *Am J Physiol Heart Circ Physiol* 288: H227–H234, 2005.
6. **Bandell M, Story GM, Hwang SW, Viswanath V, Eid SR, Petrus MJ, Earley TJ, Patapoutian A.** Noxious cold ion channel TRPA1 is activated by pungent compounds and bradykinin. *Neuron* 41: 849–857, 2004.
7. **Baynes JW, Thorpe SR.** Role of oxidative stress in diabetic complications: a new perspective on an old paradigm. *Diabetes* 48: 1–9, 1999.
8. **Beisswenger PJ, Howell SK, O'Dell RM, Wood ME, Touchette AD, Szwergold BS.** α-Dicarbonyls increase in the postprandial period and reflect the degree of hyperglycemia. *Diabetes Care* 24: 726–732, 2001.
9. **Bierhaus A, Fleming T, Stoyanov S, Leffler A, Babes A, Neacsu C, Sauer SK, Eberhardt M, Schnolzer M, Lasitschka F, Neuhuber WL, Kichko TI, Konrade I, Elvert R, Mier W, Pirags V, Lukic IK, Morcos M, Dehmer T, Rabbani N, Thornalley PJ, Edelstein D, Nau C, Forbes J, Humpert PM, Schwaninger M, Ziegler D, Stern DM, Cooper ME, Haberkorn U, Brownlee M, Reeh PW, Nawroth PP.** Methylglyoxal modification of Nav1.8 facilitates nociceptive neuron firing and causes hyperalgesia in diabetic neuropathy. *Nat Med* 18: 926–933, 2012.
10. **Boudina S, Abel ED.** Diabetic cardiomyopathy revisited. *Circulation* 115: 3213–3223, 2007.
11. **Brouwers O, Niessen PM, Haenen G, Miyata T, Brownlee M, Stehouwer CD, De Mey JG, Schalkwijk CG.** Hyperglycaemia-induced impairment of endothelium-dependent vasorelaxation in rat mesenteric arteries is mediated by intracellular methylglyoxal levels in a pathway dependent on oxidative stress. *Diabetologia* 53: 989–1000, 2010.
12. **Brown RD, Ambler SK, Mitchell MD, Long CS.** The cardiac fibroblast: therapeutic target in myocardial remodeling and failure. *Annu Rev Pharmacol Toxicol* 45: 657–687, 2005.
13. **Cao DS, Zhong L, Hsieh TH, Abooj M, Bishnoi M, Hughes L, Premkumar LS.** Expression of transient receptor potential ankyrin 1 (TRPA1) and its role in insulin release from rat pancreatic beta cells. *PLoS One* 7: e38005, 2012.
14. **Chang T, Wang R, Olson DJ, Mousseau DD, Ross AR, Wu L.** Modification of Akt1 by methylglyoxal promotes the proliferation of vascular smooth muscle cells. *FASEB J* 25: 1746–1757, 2011.
15. **Chaplen FW, Fahl WE, Cameron DC.** Evidence of high levels of methylglyoxal in cultured Chinese hamster ovary cells. *Proc Natl Acad Sci USA* 95: 5533–5538, 1998.
16. **Che W, Asahi M, Takahashi M, Kaneto H, Okado A, Higashiyama S, Taniguchi N.** Selective induction of heparin-binding epidermal growth factor-like growth factor by methylglyoxal and 3-deoxyglucosone in rat aortic smooth muscle cells. The involvement of reactive oxygen species formation and a possible implication for atherogenesis in diabetes. *J Biol Chem* 272: 18453–18459, 1997.
17. **Chen JB, Tao R, Sun HY, Tse HF, Lau CP, Li GR.** Multiple Ca^{2+} signaling pathways regulate intracellular Ca^{2+} activity in human cardiac fibroblasts. *J Cell Physiol* 223: 68–75, 2010.
18. **Chen K, Mehta JL, Li D, Joseph L, Joseph J.** Transforming growth factor beta receptor endoglin is expressed in cardiac fibroblasts and modulates profibrogenic actions of angiotensin II. *Circ Res* 95: 1167–1173, 2004.
19. **Cook LJ, Davies J, Yates AP, Elliott AC, Lovell J, Joule JA, Pemberton P, Thornalley PJ, Best L.** Effects of methylglyoxal on rat pancreatic beta-cells. *Biochem Pharmacol* 55: 1361–1367, 1998.
20. **Cruz-Orengo L, Dhaka A, Heuermann RJ, Young TJ, Montana MC, Cavanaugh EJ, Kim D, Story GM.** Cutaneous nociception evoked by 15-delta PGJ2 via activation of ion channel TRPA1. *Mol Pain* 4: 30-80697-4-30, 2008.
21. **Dai B, Cui M, Zhu M, Su WL, Qiu MC, Zhang H.** STAT1/3 and ERK1/2 synergistically regulate cardiac fibrosis induced by high glucose. *Cell Physiol Biochem* 32: 960–971, 2013.
22. **Davis J, Burr AR, Davis GF, Birnbaumer L, Molkentin JD.** A TRPC6-dependent pathway for myofibroblast transdifferentiation and wound healing in vivo. *Dev Cell* 23: 705–715, 2012.
23. **Desai K, Wu L.** Methylglyoxal and advanced glycation endproducts: new therapeutic horizons? *Recent Pat Cardiovasc Drug Discov* 2: 89–99, 2007.
24. **Dhar A, Desai K, Kazachmov M, Yu P, Wu L.** Methylglyoxal production in vascular smooth muscle cells from different metabolic precursors. *Metabolism* 57: 1211–1220, 2008.
25. **Du J, Xie J, Zhang Z, Tsujikawa H, Fusco D, Silverman D, Liang B, Yue L.** TRPM7-mediated Ca^{2+} signals confer fibrogenesis in human atrial fibrillation. *Circ Res* 106: 992–1003, 2010.
26. **Eberhardt MJ, Filipovic MR, Leffler A, de la Roche J, Kistner K, Fischer MJ, Fleming T, Zimmermann K, Ivanovic-Burmazovic I, Nawroth PP, Bierhaus A, Reeh PW, Sauer SK.** Methylglyoxal activates nociceptors through transient receptor potential channel A1 (TRPA1): a possible mechanism of metabolic neuropathies. *J Biol Chem* 287: 28291–28306, 2012.
27. **From AM, Scott CG, Chen HH.** The development of heart failure in patients with diabetes mellitus and pre-clinical diastolic dysfunction a population-based study. *J Am Coll Cardiol* 55: 300–305, 2010.
28. **Gabbiani G, Ryan GB, Majne G.** Presence of modified fibroblasts in granulation tissue and their possible role in wound contraction. *Experientia* 27: 549–550, 1971.
29. **Graham S, Gorin Y, Abboud HE, Ding M, Lee DY, Shi H, Ding Y, Ma R.** Abundance of TRPC6 protein in glomerular mesangial cells is decreased by ROS and PKC in diabetes. *Am J Physiol Cell Physiol* 301: C304–C315, 2011.
30. **Grynkiewicz G, Poenie M, Tsien RY.** A new generation of Ca^{2+} indicators with greatly improved fluorescence properties. *J Biol Chem* 260: 3440–3450, 1985.
31. **Guinamard R, Bois P.** Involvement of transient receptor potential proteins in cardiac hypertrophy. *Biochim Biophys Acta* 1772: 885–894, 2007.
32. **Harada M, Luo X, Qi XY, Tadevosyan A, Maguy A, Ordog B, Ledoux J, Kato T, Naud P, Voigt N, Shi Y, Kamiya K, Murohara T, Kodama I, Tardif JC, Schotten U, Van Wagoner DR, Dobrev D, Nattel S.** Transient receptor potential canonical-3 channel-dependent fibroblast regulation in atrial fibrillation. *Circulation* 126: 2051–2064, 2012.
33. **Heymes C, Vanderheyden M, Bronzwaer JG, Shah AM, Paulus WJ.** Endomyocardial nitric oxide synthase and left ventricular preload reserve in dilated cardiomyopathy. *Circulation* 99: 3009–3016, 1999.
34. **Huang W, Rubinstein J, Prieto AR, Wang DH.** Enhanced postmyocardial infarction fibrosis via stimulation of the transforming growth factor-beta-Smad2 signaling pathway: role of transient receptor potential vanilloid type 1 channels. *J Hypertens* 28: 367–376, 2010.
35. **Ikeda K, Nakajima T, Yamamoto Y, Takano N, Tanaka T, Kikuchi H, Oguri G, Morita T, Nakamura F, Komuro I.** Roles of transient receptor potential canonical (TRPC) channels and reverse-mode Na^+/Ca^{2+} exchanger on cell proliferation in human cardiac fibroblasts: effects of transforming growth factor beta1. *Cell Calcium* 54: 213–225, 2013.
36. **Inoue R, Jensen LJ, Shi J, Morita H, Nishida M, Honda A, Ito Y.** Transient receptor potential channels in cardiovascular function and disease. *Circ Res* 99: 119–131, 2006.
37. **Jia X, Chang T, Wilson TW, Wu L.** Methylglyoxal mediates adipocyte proliferation by increasing phosphorylation of Akt1. *PLoS One* 7: e36610, 2012.
38. **Jordt SE, Bautista DM, Chuang HH, McKemy DD, Zygmunt PM, Hogestatt ED, Meng ID, Julius D.** Mustard oils and cannabinoids excite sensory nerve fibres through the TRP channel ANKTM1. *Nature* 427: 260–265, 2004.
39. **Kakkar R, Lee RT.** Intramyocardial fibroblast myocyte communication. *Circ Res* 106: 47–57, 2010.
40. **Karashima Y, Talavera K, Everaerts W, Janssens A, Kwan KY, Vennekens R, Nilius B, Voets T.** TRPA1 acts as a cold sensor in vitro and in vivo. *Proc Natl Acad Sci USA* 106: 1273–1278, 2009.
41. **Kelly DJ, Zhang Y, Connelly K, Cox AJ, Martin J, Krum H, Gilbert RE.** Tranilast attenuates diastolic dysfunction and structural injury in experimental diabetic cardiomyopathy. *Am J Physiol Heart Circ Physiol* 293: H2860–H2869, 2007.

42. **Koch SE, Gao X, Haar L, Jiang M, Lasko VM, Robbins N, Cai W, Brokamp C, Varma P, Tranter M, Liu Y, Ren X, Lorenz JN, Wang HS, Jones WK, Rubinstein J.** Probenecid: novel use as a non-injurious positive inotrope acting via cardiac TRPV2 stimulation. *J Mol Cell Cardiol* 53: 134–144, 2012.
43. **Kumaran C, Shivakumar K.** Calcium- and superoxide anion-mediated mitogenic action of substance P on cardiac fibroblasts. *Am J Physiol Heart Circ Physiol* 282: H1855–H1862, 2002.
44. **Kuwahara K, Wang Y, McAnally J, Richardson JA, Bassel-Duby R, Hill JA, Olson EN.** TRPC6 fulfills a calcineurin signaling circuit during pathologic cardiac remodeling. *J Clin Invest* 116: 3114–3126, 2006.
45. **Lapolla A, Flamini R, Dalla Vedova A, Senesi A, Reitano R, Fedele D, Basso E, Seraglia R, Traldi P.** Glyoxal and methylglyoxal levels in diabetic patients: quantitative determination by a new GC/MS method. *Clin Chem Lab Med* 41: 1166–1173, 2003.
46. **Lo TW, Selwood T, Thornalley PJ.** The reaction of methylglyoxal with aminoguanidine under physiological conditions and prevention of methylglyoxal binding to plasma proteins. *Biochem Pharmacol* 48: 1865–1870, 1994.
47. **Minke B, Cook B.** TRP channel proteins and signal transduction. *Physiol Rev* 82: 429–472, 2002.
48. **Mukherjee S, Kolb MR, Duan F, Janssen LJ.** Transforming growth factor-beta evokes Ca^{2+} waves and enhances gene expression in human pulmonary fibroblasts. *Am J Respir Cell Mol Biol* 46: 757–764, 2012.
49. **Mukhopadhyay I, Gomes P, Aranake S, Shetty M, Karnik P, Damle M, Kuruganti S, Thorat S, Khairatkar-Joshi N.** Expression of functional TRPA1 receptor on human lung fibroblast and epithelial cells. *J Recept Signal Transduct Res* 31: 350–358, 2011.
50. **Mukohda M, Yamawaki H, Nomura H, Okada M, Hara Y.** Methylglyoxal inhibits smooth muscle contraction in isolated blood vessels. *J Pharmacol Sci* 109: 305–310, 2009.
51. **Nagata K, Duggan A, Kumar G, Garcia-Anoveros J.** Nociceptor and hair cell transducer properties of TRPA1, a channel for pain and hearing. *J Neurosci* 25: 4052–4061, 2005.
52. **Nakajima T, Okuda Y, Chisaki K, Shin WS, Iwasawa K, Morita T, Matsumoto A, Suzuki JI, Suzuki S, Yamada N, Toyo-Oka T, Nagai R, Omata M.** Bile acids increase intracellular Ca^{2+} concentration and nitric oxide production in vascular endothelial cells. *Br J Pharmacol* 130: 1457–1467, 2000.
53. **Ohkawara S, Tanaka-Kagawa T, Furukawa Y, Jinno H.** Methylglyoxal activates the human transient receptor potential ankyrin 1 channel. *J Toxicol Sci* 37: 831–835, 2012.
54. **Porter KE, Turner NA.** Cardiac fibroblasts: at the heart of myocardial remodeling. *Pharmacol Ther* 123: 255–278, 2009.
55. **Redfield MM, Jacobsen SJ, Burnett JC, Jr Mahoney DW, Bailey KR, Rodeheffer RJ.** Burden of systolic and diastolic ventricular dysfunction in the community: appreciating the scope of the heart failure epidemic. *JAMA* 289: 194–202, 2003.
56. **Shao CH, Capek HL, Patel KP, Wang M, Tang K, DeSouza C, Nagai R, Mayhan W, Periasamy M, Bidasee KR.** Carbonylation contributes to SERCA2a activity loss and diastolic dysfunction in a rat model of type 1 diabetes. *Diabetes* 60: 947–959, 2011.
57. **Stahrenberg R, Edelmann F, Mende M, Kockskamper A, Dungen HD, Scherer M, Kochen MM, Binder L, Herrmann-Lingen C, Schonbrunn L, Gelbrich G, Hasenfuss G, Pieske B, Wachter R.** Association of glucose metabolism with diastolic function along the diabetic continuum. *Diabetologia* 53: 1331–1340, 2010.
58. **Stokes A, Wakano C, Koblan-Huberson M, Adra CN, Fleig A, Turner H.** TRPA1 is a substrate for de-ubiquitination by the tumor suppressor CYLD. *Cell Signal* 18: 1584–1594, 2006.
59. **Story GM, Peier AM, Reeve AJ, Eid SR, Mosbacher J, Hricik TR, Earley TJ, Hergarden AC, Andersson DA, Hwang SW, McIntyre P, Jegla T, Bevan S, Patapoutian A.** ANKTM1, a TRP-like channel expressed in nociceptive neurons, is activated by cold temperatures. *Cell* 112: 819–829, 2003.
60. **Suskin N, McKelvie RS, Burns RJ, Latini R, Pericak D, Probstfield J, Rouleau JL, Sigouin C, Solymoss CB, Tsuyuki R, White M, Yusuf S.** Glucose and insulin abnormalities relate to functional capacity in patients with congestive heart failure. *Eur Heart J* 21: 1368–1375, 2000.
61. **Tang M, Zhang W, Lin H, Jiang H, Dai H, Zhang Y.** High glucose promotes the production of collagen types I and III by cardiac fibroblasts through a pathway dependent on extracellular-signal-regulated kinase 1/2. *Mol Cell Biochem* 301: 109–114, 2007.
62. **Thornalley PJ, Hooper NI, Jennings PE, Florkowski CM, Jones AF, Lunec J, Barnett AH.** The human red blood cell glyoxalase system in diabetes mellitus. *Diabetes Res Clin Pract* 7: 115–120, 1989.
63. **van Heerebeek L, Hamdani N, Handoko ML, Falcao-Pires I, Musters RJ, Kupreishvili K, Ijsselmuiden AJ, Schalkwijk CG, Bronzwaer JG, Diamant M, Borbely A, van der Velden J, Stienen GJ, Laarman GJ, Niessen HW, Paulus WJ.** Diastolic stiffness of the failing diabetic heart: importance of fibrosis, advanced glycation end products, and myocyte resting tension. *Circulation* 117: 43–51, 2008.
64. **Wahl M, Gruenstein E.** Intracellular free Ca^{2+} in the cell cycle in human fibroblasts: transitions between G1 and G0 and progression into S phase. *Mol Biol Cell* 4: 293–302, 1993.
65. **Wang H, Meng QH, Gordon JR, Khandwala H, Wu L.** Proinflammatory and proapoptotic effects of methylglyoxal on neutrophils from patients with type 2 diabetes mellitus. *Clin Biochem* 40: 1232–1239, 2007.
66. **Wang P, Li HW, Wang YP, Chen H, Zhang P.** Effects of recombinant human relaxin upon proliferation of cardiac fibroblast and synthesis of collagen under high glucose condition. *J Endocrinol Invest* 32: 242–247, 2009.
67. **Wang X, Chang T, Jiang B, Desai K, Wu L.** Attenuation of hypertension development by aminoguanidine in spontaneously hypertensive rats: role of methylglyoxal. *Am J Hypertens* 20: 629–636, 2007.
68. **Wang X, Desai K, Chang T, Wu L.** Vascular methylglyoxal metabolism and the development of hypertension. *J Hypertens* 23: 1565–1573, 2005.
69. **Wang YJ, Sung RJ, Lin MW, Wu SN.** Contribution of BK_{Ca}-channel activity in human cardiac fibroblasts to electrical coupling of cardiomyocytes-fibroblasts. *J Membr Biol* 213: 175–185, 2006.
70. **Wang YY, Chang RB, Waters HN, McKemy DD, Liman ER.** The nociceptor ion channel TRPA1 is potentiated and inactivated by permeating calcium ions. *J Biol Chem* 283: 32691–32703, 2008.
71. **Weber KT.** Fibrosis in hypertensive heart disease: focus on cardiac fibroblasts. *J Hypertens* 22: 47–50, 2004.
72. **Wu X, Eder P, Chang B, Molkentin JD.** TRPC channels are necessary mediators of pathologic cardiac hypertrophy. *Proc Natl Acad Sci USA* 107: 15: 7000–7005, 2010.
73. **Wuensch T, Thilo F, Krueger K, Scholze A, Ristow M, Tepel M.** High glucose-induced oxidative stress increases transient receptor potential channel expression in human monocytes. *Diabetes* 59: 4: 844–849, 2010.
74. **Yuen A, Laschinger C, Talior I, Lee W, Chan M, Birek J, Young EW, Sivagurunathan K, Won E, Simmons CA, McCulloch CA.** Methylglyoxal-modified collagen promotes myofibroblast differentiation. *Matrix Biol* 29: 6: 537–548, 2010.
75. **Zhao Y, Huang H, Jiang Y, Wei H, Liu P, Wang W, Niu W.** Unusual localization and translocation of TRPV4 protein in cultured ventricular myocytes of the neonatal rat. *Eur J Histochem* 56: 3: e32, 2012.

resulted in an overestimation of the expected number of deaths from colorectal cancer in the background population and an underestimation of the risk in the screening cohort. Taking this into account, their results would show a standardized incidence rate ratio of colorectal cancer of between 0.7 and 1.4 (with lead-time estimates between 5 years and 1 year), which is in line with the rate in our study.

Both de Groen et al. and Winawer emphasize the quality of colonoscopy as a determinant for a reduction in the risk of colorectal cancer. Our study did not include information on the quality of colonoscopy, but it is derived from a large sample in a country with a national colonoscopy quality-assurance program.[1] Thus, our study should facilitate valid estimates for what can be achieved in routine colonoscopies.

Winawer correctly notes that surveillance in patients with high-risk adenomas seems more compelling than surveillance in patients with low-risk adenomas. However, we agree with Haug and Senore that the observed 16% excess risk of death from colorectal cancer in the high-risk group (with the very limited surveillance applied in the study) is modest. On the basis of the results of our sample study, we further think that the real risk in fact may even be lower in both the high-risk group and the low-risk group, because more detailed polyp classification would have moved the adenomas with the highest risk in the low-risk group to the high-risk group, resulting in a lower risk in both groups. This is what is commonly referred to as the "Will Rogers phenomenon."[2] Indeed, our findings of only a slightly increased risk of death from colorectal cancer among high-risk patients and no increased risk among low-risk patients call for a critical review of current recommendations for surveillance. It is worthwhile to consider the prioritization of screening colonoscopy for everybody instead of the use of large resources for intensive surveillance after adenoma removal. A large-scale randomized trial investigating various surveillance intervals after adenoma removal is scheduled to start in Europe in 2015.[3]

Michael Bretthauer, M.D., Ph.D.
Magnus Løberg, M.D.
Mette Kalager, M.D., Ph.D.
University of Oslo
Oslo, Norway

Since publication of their article, the authors report no further potential conflict of interest.

1. Gastronet home page. Oslo: Cancer Registry of Norway (http://www.kreftregisteret.no/no/Forskning/Prosjekter/Gastronet).
2. Feinstein AR, Sosin DM, Wells CK. The Will Rogers phenomenon: stage migration and new diagnostic techniques as a source of misleading statistics for survival in cancer. N Engl J Med 1985;312:1604-8.
3. EPoS (European Polyp Surveillance) study. Oslo: Institute of Health and Society (http://www.med.uio.no/helsam/english/research/projects/epos/index.html).

DOI: 10.1056/NEJMc1411954

Somatic Mutations in Cerebral Cortical Malformations

TO THE EDITOR: Jamuar et al. (Aug. 21 issue)[1] showed that targeted high-coverage sequencing is useful in detecting somatic mutations in etiologic genes in DNA obtained from the leukocytes of patients with cerebral cortical malformations. They observed that five of the eight mosaic mutations detected with high-coverage sequencing had been missed by Sanger sequencing because of their low prevalence. The phenotype of disease caused by a mosaic variant was typically milder than that caused by the identical variant occurring as a germline mutation. At what point does the low somatic prevalence of a mutation that has an established cause (when constitutive) render the mutation nonetiologic? Presumably, there is a threshold under which the mutation does not place a burden on the biology of the nervous system. Could any "pathogenic" mosaic variant with a very low prevalence — that may not reach the threshold of pathogenicity — be incidentally detected in healthy control persons?

Hiroyuki Morita, M.D., Ph.D.
Issei Komuro, M.D., Ph.D.
University of Tokyo
Tokyo, Japan
hmrt-tky@umin.net

No potential conflict of interest relevant to this letter was reported.

1. Jamuar SS, Lam AT, Kircher M, et al. Somatic mutations in cerebral cortical malformations. N Engl J Med 2014;371:733-43.

DOI: 10.1056/NEJMc1411784

THE AUTHORS REPLY: Morita and Komuro suggest that pathogenic mosaic variants reported in our study, with a very low allele frequency, may perhaps be incidental rather than pathogenic. We did not sequence unaffected control persons but imagine that they might show mutations at low levels of mosaicism. For example, targeted deep sequencing of *PIK3CA* of healthy persons[1] showed a mean mutant allele frequency of 0.2×10^{-4} to 19×10^{-4}, which does not exceed the expected allele frequency of sequencing-related errors (0.1 substitutions per 100 bases)[2] and is lower than the lowest level of mosaicism detected in our study (5%). Other research groups have reported mosaicism of etiologic mutations as low as 1% in leukocyte-derived DNA of persons with brain malformation[1] and 4.2% in the DNA of persons with neonatal-onset multisystem inflammatory disease.[3] In addition, as described in the article and illustrated in Figure S5 in the Supplementary Appendix (available with the full text of our article at NEJM.org), when we compared rates of neutral and deleterious mutations according to disease category, we observed a highly significant association between deleterious mutations and the diagnosis to which they were specific, and no such association with neutral variants (i.e., these had similar allele frequencies across the different disorders). These data support causal roles for the reported mutations and argue against their being incidental findings.

Saumya S. Jamuar, M.B., B.S.
KK Women's and Children's Hospital
Singapore, Singapore
Christopher A. Walsh, M.D., Ph.D.
Boston Children's Hospital
Boston, MA
christopher.walsh@childrens.harvard.edu

Since publication of their article, the authors report no further potential conflict of interest.

1. Rivière J-B, Mirzaa GM, O'Roak BJ, et al. De novo germline and postzygotic mutations in AKT3, PIK3R2 and PIK3CA cause a spectrum of related megalencephaly syndromes. Nat Genet 2012;44:934-40.
2. Loman NJ, Misra RV, Dallman TJ, et al. Performance comparison of benchtop high-throughput sequencing platforms. Nat Biotechnol 2012;30:434-9.
3. Tanaka N, Izawa K, Saito MK, et al. High incidence of NLRP3 somatic mosaicism in patients with chronic infantile neurologic, cutaneous, articular syndrome: results of an International Multicenter Collaborative Study. Arthritis Rheum 2011;63:3625-32.

DOI: 10.1056/NEJMc1411784

A Molecular Basis for Nicotine as a Gateway Drug

TO THE EDITOR: In their Shattuck Lecture (Sept. 4 issue),[1] Kandel and Kandel share evidence of a biochemical basis by which the use of nicotine enhances the addictive potential of cocaine. The experiments they report measured addiction-related behaviors and molecular markers of addiction in mice. However, before we conclude that nicotine is a biochemical gateway drug, it is important to compare the effect size of the biochemical properties of nicotine against the enormity and ubiquity of social factors associated with tobacco products.

Whether tobacco use is causal of, or only associated with, future drug use remains a central question. Kandel and Kandel present compelling molecular evidence in mice, but experiments involving humans are necessary to address the social confounders of tobacco use. An experiment to address this question would be to compare rates of cocaine addiction at the more than 1477 smoke-free college and university campuses in the United States before the implementation of such policies with rates after implementation.[2]

Jacob M. Rosenberg, Sc.B.
Stanford University School of Medicine
Stanford, CA
jakeros@stanford.edu

No potential conflict of interest relevant to this letter was reported.

1. Kandel ER, Kandel DB. Shattuck Lecture: a molecular basis for nicotine as a gateway drug. N Engl J Med 2014;371:932-43.
2. Smokefree and tobacco-free U.S. and tribal colleges and universities. Berkeley, CA: American Nonsmokers' Rights Foundation, 2014 (http://no-smoke.org/pdf/smokefreecollegesuniversities.pdf).

DOI: 10.1056/NEJMc1411785

THE AUTHORS REPLY: Rosenberg is correct that in humans, social factors play an important role in the use of drugs. This is one of the key rea-

ORIGINAL RESEARCH

American Heart Association | American Stroke Association.

Anti-Inflammatory Peptides From Cardiac Progenitors Ameliorate Dysfunction After Myocardial Infarction

Mei-Lan Liu, MD, PhD; Toshio Nagai, MD, PhD; Masakuni Tokunaga, MD, PhD; Koji Iwanaga, MD, PhD; Katsuhisa Matsuura, MD, PhD; Toshinao Takahashi, MD, PhD; Masato Kanda, MD, PhD; Naomichi Kondo, MD, PhD; Atsuhiko T. Naito, MD, PhD; Issei Komuro, MD, PhD; Yoshio Kobayashi, MD, PhD

Background—Cardiac cell therapy has been proposed as one of the new strategies against myocardial infarction. Although several reports showed improvement of the function of ischemic heart, the effects of cell therapy vary among the studies and the mechanisms of the beneficial effects are still unknown. Previously, we reported that clonal stem cell antigen-1–positive cardiac progenitor cells exerted a therapeutic effect when transplanted into the ischemic heart. Our aims were to identify the cardiac progenitor-specific paracrine factor and to elucidate the mechanism of its beneficial effect.

Methods and Results—By using an antibody array, we found that soluble junctional adhesion molecule-A (JAM-A) was abundantly secreted from cardiac progenitor cells. Pretreatment of neutrophils with conditioned medium from cultured cardiac progenitor cells or soluble JAM-A inhibited transendothelial migration and reduced motility of neutrophils. These inhibitory effects were attenuated by anti–JAM-A neutralizing antibody. Injection of cardiac progenitor cells into infarct heart attenuated neutrophil infiltration and expression of inflammatory cytokines. Injection of soluble JAM-A–expressing, but not of JAM-A siRNA–expressing, cardiac progenitor cells into the infarct heart prevented cardiac remodeling and reduced fibrosis area.

Conclusions—Soluble JAM-A secreted from cardiac progenitor cells reduces infiltration of neutrophils after myocardial infarction and ameliorates tissue damage through prevention of excess inflammation. Our finding may lead to a new therapy for cardiovascular disease by using the anti-inflammatory effect of JAM-A. (***J Am Heart Assoc.* 2014;03:e001101 doi: 10.1161/JAHA.114.001101**)

Key Words: cardiac progenitor cells • cell adhesion molecules • cell transplantation • inflammation • myocardial infarction

Many randomized controlled clinical trials have demonstrated that cell therapy improves the function of ischemic heart. However, the results are inconsistent among the trials. One reason for improvement is said to be procedure-related variables. Thus, the establishment of optimal protocol regarding to the cell source, timing of transplantation, and delivery methods is awaited.[1,2] In addition to these technical issues, it has been recognized that an understanding of the mechanism of action is important to overwhelm the current limitation of cell therapy. Recently, the secretion of factors with paracrine effects by the transplanted cells has been considered as one of the mechanisms of the beneficial effects of cell therapy.[3] Previously, we reported that among cardiac progenitor cells, bone marrow mononuclear cells (BMs), skeletal myoblasts (SMs), and adipose tissue–derived mesenchymal cells (AMCs), transplantation of cardiac progenitor cells (CPCs) most effectively prevents cardiac remodeling and dysfunction.[4] The superior effect of CPC transplantation was based on both transdifferentiation of transplanted cells and paracrine mechanism. Recently, we have identified soluble vascular cell adhesion molecule 1 (VCAM-1), which was secreted in a large amount from CPCs but not AMCs, attenuate cardiac remodeling after myocardial infarction (MI) through the promotion of angiogenesis and survival of cardiomyocytes.[5] Various types of cells, such as BMs, SMs, AMCs, and CPCs, secrete many kinds of distinct proteins according to their organ-specific profile. Therefore, it is conceivable that comprehensive analysis of secreted proteins from different cell sources may help us to find a new paracrine factor that can ameliorate cardiac function through

From the Department of Cardiovascular Medicine Chiba, University Graduate School of Medicine, Chuo-ku, Chiba, Japan (M-L.L., T.N., M.T., K.I., T.T., M.K., N.K., Y.K.); Department of Cardiology and Institute of Advanced Biomedical Engineering and Science, Tokyo Women's Medical University, Shinjuku-ku, Tokyo, Japan (K.M.); Department of Cardiovascular Medicine, The University of Tokyo Graduate School of Medicine, Tokyo, Japan (A.T.N., I.K.).

Correspondence to: Toshio Nagai, MD, PhD, Department of Cardiovascular Medicine, Chiba University Graduate School of Medicine, 1-8-1 Inohana, Chuo-ku, Chiba 260-8670 Japan. E-mail: toshi35526@yahoo.co.jp

cytoprotective and angiogenic potential or even some unidentified mechanisms.

We analyzed secreted proteins from CPCs, BMs, SMs, and AMCs by using a cytokine antibody array. Among 144 cytokines, we identified that junctional adhesion molecule-A (JAM-A), VCAM-1, and granulocyte-colony stimulating factor were exclusively released from CPCs. JAM-A is a component of the junction of epithelial and endothelial cells, and recently it was reported that the soluble form of JAM-A regulates transendothelial migration of leukocytes.[6] We examined the potential mechanism of CPC transplantation from the facet of JAM-A–mediated anti-inflammatory effect by using a mouse MI model.

Methods

Animals

Wild-type mice (C57Bl/6J, 10 to 12 weeks) were purchased from Japan SLC. All protocols were approved by the Institutional Animal Care and Use Committee of Chiba University Graduate School of Medicine and the Japanese Government Animal Protection and Management Law (No. 105).

Preparation of Cells

CPCs are clonal cells established from adult mouse heart stem cell antigen-1–positive cells as described previously.[4,7] CPCs were cultured in Iscove's modified Dulbecco's medium (Life Technologies) with 10% FBS and passaged before reaching confluence. AMCs were isolated from adult mice as described previously with a few modifications.[8] Briefly, white adipose tissues were digested at 37°C in PBS with 2.5 mg/mL Dispase (Life Technologies) for 45 minutes. After filtration through 25-μm filters and centrifugation, isolated AMCs were suspended in DMEM (Sigma-Aldrich) supplemented with 10% FBS and penicillin-streptomycin and cultured on 1% gelatin-coated dishes. AMCs after passages 3 to 5 were used. SMs were isolated from the hindlimbs of adult mice as described previously.[9] In brief, minced muscle tissues were digested in 0.05% trypsin-EDTA and cultured in F-10 medium (Life Technologies) with 20% horse serum and 2.5 ng/mL basic fibroblast growth factor (Promega) for 4 days. SMs were expanded in the medium with 20% FBS and used within 2 or 3 passages. BMs were harvested from adult mice. Mononuclear cells were subsequently separated by using Histopaque 1083 (Sigma-Aldrich), suspended in Iscove's modified Dulbecco's medium.

Neonatal rat cardiomyocytes were isolated as previously described.[10] Cardiomyocytes were plated at a field density of 1×10^6 cells/cm^2 on 10-cm culture dishes (BD Biosciences) and cultured in DMEM supplemented with 10% FBS. To obtain a chemotactic condition medium, cardiomyocytes were exposed to 12 hours of hypoxia (<0.1% O_2 5% CO_2–95% N_2) in serum-free DMEM without glucose.

Animal Surgery and Cell Transplantation

The mice were anesthetized via intraperitoneal injection of 50 mg/kg sodium pentobarbital and ventilated with use of a volume-regulated respirator. MI was produced through ligation of the left anterior descending coronary artery with a 10-0 Prolene suture. Transplantation of CPCs and self-assembling nanopeptide (Puramatrix™ [PM] kindly provided from 3-D Matrix, Ltd) was performed as previously described.[4] Briefly, 10 μL of 0.1% PM-CPC mixture containing 2×10^4 cells was directly injected into the border zone of infarct myocardium 2 times just after ligation of the coronary artery. Subsequently, 20 μL of 0.5% PM-CPC mixture containing 2×10^4 cells was disseminated onto the surface of infarct area. To deliver soluble JAM-A protein into the heart tissue, 0.25 μg/μL recombinant mouse JAM-A Fc chimera (JAM-A Fc; R&D Systems) was mixed with PM and transplanted in the same way as the CPCs. The final concentration of JAM-A Fc in PM was 25 μg/mL. To detect the transplanted CPCs, they were infected with red fluorescent protein (RFP)-expressing retroviral vector as described previously.[4]

Cytokine Antibody Array

CPCs, AMCs, and SMs (1.0×10^6) were seeded onto 10-cm dishes. After incubation for 12 hours in the appropriate medium supplemented with 10% FBS, cells were thoroughly washed with PBS 3 times and medium was changed to serum-depleted DMEM. Isolated BMs (1.0×10^6) were seeded onto 10-cm dishes with serum-depleted Iscove's modified Dulbecco's medium. After incubation for 24 hours in serum-depleted medium, the supernatant was collected as conditioned medium (CM) and the contaminating cells were removed via centrifuge. The released cytokine was measured by using Mouse Cytokine Antibody Array (RayBiotech Inc and R&D Systems). The expression level of each cytokines was quantified by using Gene Pix 4000B (Molecular Devices, Inc).

Neutrophils Migration Assay

Human umbilical vein endothelial cells (HUVECs) (6×10^5) were seeded onto 1% gelatin–coated transwell culture inserts with 3-μm pores (Corning) and grown for 2 days in 5% CO_2 at 37°C. Human polymorphonuclear leukocytes were isolated as previously described.[11] Briefly, whole blood was obtained from healthy laboratory volunteers. Leukocytes were separated from whole blood through dextran sedimentation and lysis of contaminating erythrocytes. Neutrophils were further

purified by using Ficoll (Sigma-Aldrich) density gradient centrifugation. Isolated neutrophils were preincubated with either 10 μg/mL JAM-A Fc, 5 mL of CPC CM, or 5 mL of CPC CM with 1 μg/mL neutralizing anti-mouse JAM-A antibody (R&D Systems) for 30 minutes, washed, and added to the upper chamber (5×10^5 cells in RPMI medium with 0.2% BSA). A chemotactic gradient was created by the addition of 40 ng/mL tumor necrosis factor-α (TNFα; R&D Systems) or hypoxic cardiomyocytes CM to the lower chamber. After 3 hours of incubation, transmigrated cells in the lower chamber were counted by using a hematocytometer.

For the assay of the length of neutrophil tails, neutrophils were purified from bone marrow by using EASYSEP (BD Pharmingen) according to the manufacture's instruction. After preincubation with either 10 μg/mL JAM-A Fc, CPC CM, or CPC CM with 1 μg/mL neutralizing anti-mouse JAM-A antibody for 30 minutes, neutrophils (0.4×10^6 cells) were seeded onto fibronectin-coated (20 μg/mL in PBS) coverslips for 10 minutes at 37°C followed by additional incubation with 5 nmol/L WKYMVm (Merck Millipore) for 20 minutes at 37°C. Cells were fixed with 4% paraformaldehyde for 20 minutes at room temperature and permeabilized with 1% NP-40 for 5 minutes. Actin was stained with rhodamine phalloidin (Life Technologies). Images were taken made with fluorescent microscopy (Axioskop 40; Carl Zeiss), the length of neutrophil tails was measured by using Adobe Photoshop software version 12.0 for Macintosh (Adobe Systems), and the frequency of cells with different tail size was examined.

Morphological Examination and Immunohistochemistry

The transversal sections (4 μm) from paraffin embedded formalin fixed tissue were subjected to Masson's trichrome staining. Fibrous infarct area was measured as described previously.[4] The paraffin sections were stained with anti–von Willebrand factor (vWF) (DAKO), and the detection of antibodies was performed by using VECSTATIN ABC kit (Vector Laboratories Inc) according to the manufacturer's instruction. Nuclei were stained with hematoxylin. For fluorescent immunohistochemistry, fresh frozen sections were fixed with 4% paraformaldehyde, treated with 0.1% NP-40 and 2% BSA in PBS, and stained with anti–Ly-6G (BD Pharmingen) or anti-myeloproxidase (MPO) (Abcam) antibody. For the detection of JAM-A, CD31, and Sca-1, fresh frozen sections were fixed with chilled acetone, treated with 10% donkey serum in PBS and stained with anti–JAM-A (Hycult Biotech), anti-CD31 (BD Pharmingen), or anti–Sca-1 (Ly6A/E, BD Pharmingen) antibody. For the detection of RFP-positive cardiomyocytes, the isolated hearts were perfused and fixed with PLP (periodate lysine paraformaldehyde) Solution Set (Wako) before being frozen and then costained with anti-RFP antibody (MBL) and anti–sarcomeric α-actinin antibody (Sigma-Aldrich). Antibodies were detected appropriate fluorescent conjugated secondary antibodies (Life Technologies or Jackson Immunoresearch Laboratory). Nuclei were stained with Hochst33342 (Sigma-Aldrich). Images were taken with the use of bright field and fluorescent microscopy (Axioskop 40; Carl Zeiss). JAM-A and CD31 immunofluorescence in the border and infarct areas were analyzed by using Adobe Photoshop software version 12.0.

Picrosirius Red Staining and Collagen Matrix Quality

Paraffin sections were deparaffinized and stained by using the Picrosirius Red Stain Kit (Polysciences, Inc) according to the manufacturer's instructions. The images of myocardial scar area were obtained through microscopy (Axioskop 40) with a polarizer filter to quantify thick, tightly packed collagen fibers as yellow-red and thin, loosely assembled, immature fibers as green.[12] The images were analyzed with the use of ImageJ software (National Institutes of Health) based on the hue component of the images, and the numbers of red, orange, yellow, and green pixels were calculated.[13]

Echocardiography

Echocardiography in spontaneous breathing mice was performed by using a Vevo770 (Visual Sonics) with a 25-MHz imaging transducer. Two-dimensional images and M-mode tracing were recorded from the parasternal long-axis view at midpapillary level to determine left ventricular internal diastole diameter (LVIDD) and left ventricular internal systolic diameter (LVISD). LV fractional shortening (FS) was calculated as $\%FS=[(LVIDD-LVISD)/LVIDD]\times100$.

Dihydroethidium Fluorescence Analysis

The frozen sections (4 μm thick) were prepared and stained with 10 μmol/L dihydroethidium (DHE) in Krebs-HEPES buffer composed of (in mmol/L) 99.01 NaCl, 4.69 KCl, 1.87 $CaCl_2$, 1.20 $MgSO_4$, 1.03 $K2HPO_4$, 25.0 $NaHCO_3$, 20.0 Na-HEPES, and 11.1 glucose (pH 7.4) at 37°C for 30 minutes in a dark. The intensities of fluorescence were quantitatively analyzed with the use of Adobe Photoshop software version 12.0 for Macintosh.

Quantitative Real-Time PCR

Total RNA extraction and DNase treatment were performed by using SV total RNA Isolation Kit (Promega). RNA was DNase treated and reverse transcribed by using QuantiTect Reverse Transcription Kit (Qiagen). Real-time quantitative PCR was

Table 1. Primer Sequences and Universal Probe Library UPL Number

	Forward	Reverse	UPL No.
Mouse 28S rRNA	agcgacactcggacttgc	cgaaggactccacaggtttt	109
Ly6G	ttgtggtcctactgtgtgcag	ggtgggaccccaatacaat	19
Myeroperoxidase	ggaaggagacctagaggttgg	tagcacaggaaggccaatg	7
Cxcl1	agactccagccacactccaa	tgacagcgcagctcattg	83
Cxcl2	cagaaaatcatccaaaagatactgaa	ctttggttcttccgttgagg	26
Cxcl3	ccccaggcttcagataatca	gggatggatcgcttttctc	69
Ccl3	caagtcttctcagcgccata	ggaatcttccggctgtagg	40
Interleukin-1β	tgtaatgaaagacggcacacc	tcttctttgggtattgcttgg	78
Interleukin-6	gctaccaaactggatataatcagga	ccaggtagctatggtactccagaa	6
Interleukin-10	cagagccacatgctcctaga	tgtccagctggtcctttgtt	41
TNFα	tcttctcattcctgcttgtgg	ggtctgggccatagaactga	49

TNF indicates tumor necrosis factor; UPL, Universal Probe Library.

performed by using Universal Probe Library (UPL) (Roche Molecular Diagnostics) and Light Cycler TaqMan Master kit (Roche). Relative levels of gene expression were normalized to the mouse 28S rRNA expression by using the delta delta CT method according to the manufacturer's instructions and shown as fold increase to sham-operated mouse. Primer sequences and UPL number were listed in Table 1.

Knockdown of JAM-A Gene

Stealth small interfering RNA (siRNA) against mouse JAM-A was designed and purchased from Invitrogen. The sequence for siRNA was agugaaugaagaauucaugaaggcc. Negative controls for siRNA were purchased from Life Technologies. Transfection of siRNA was performed by using Lipofectamine RNAiMax (Life Technologies). Knockdown of *JAM-A* gene and reduction of JAM-A secretion were validated by using quantitative real-time PCR and ELISA (R&D Systems), respectively (Figure 1).

Flow Cytometry

Cells were isolated from individual hearts as previously described. Briefly, the heart was rapidly removed, minced, and then digested for 20 minutes with prewarmed buffer containing

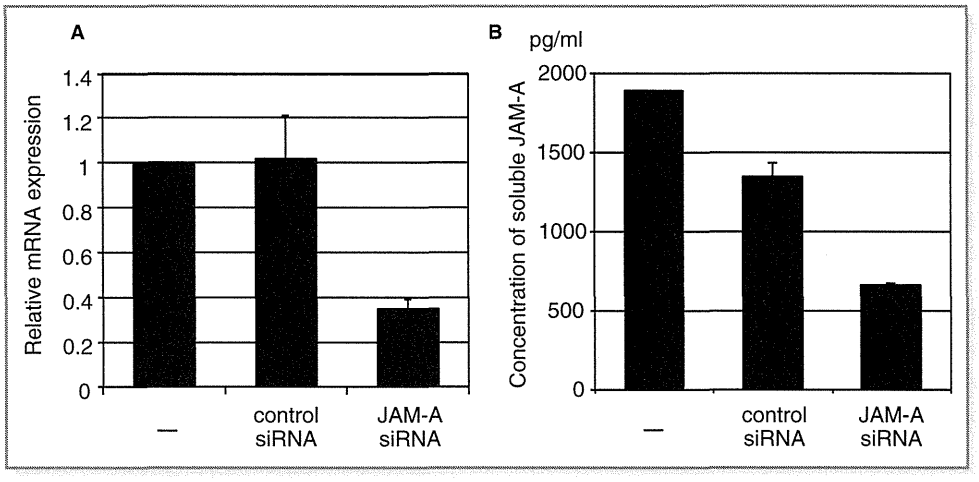

Figure 1. Validation of siRNA-mediated knockdown of JAM-A in CPC. A, Relative *JAM-A* mRNA expression in JAM-A siRNA–transfected CPC. RNA was collected from the cells 3 days after JAM-A siRNA transfection (means±SE of duplicate samples). The results shown are representative of those from 3 independent experiments. B, Concentration of soluble JAM-A in CPC CM. CM was collected from the cells 3 days after JAM-A siRNA transfection (mean±SEM of duplicate samples). Nontransfected CPCs (—) and CPCs transfected with RNAi negative control were shown as control. CM indicates conditioned medium; CPC, cardiac progenitor cells; JAM-A, junctional adhesion molecule-A; siRNA, small interfering RNA.

Table 2. Results of Cytokine Antibody Array

CPCs to BMs			CPCs to AMCs			CPCs to SMs		
Cytokine	Ratio of Net Intensity		Cytokine	Ratio of Net Intensity		Cytokine	Ratio of Net Intensity	
Decorin	289.94	243.61	VCAM-1	53.72	2.48	JAM-A	16.06	25.04
MCP-1	32.02	18.98	JAM-A	20.64	3.01	VCAM-1	10.37	3.40
TWEAK R	24.61	8.25	GCSF	2.61	7.49	Pentraxin 3	8.34	3.04
Growth arrest specific 1	16.68	20.56				GCSF	5.86	3.36
MFG-E8	13.57	27.83				GITR ligand	3.96	3.79
TIMP-1	11.63	9.96				IL-6R	2.01	3.06
VEGF	11.43	13.87						
VCAM-1	9.13	9.64						
JAM-A	6.62	10.99						
Galectin-1	6.09	4.20						
GITR Ligand	5.59	8.92						
GCSF	4.94	2.59						
sTNF RI	3.87	5.09						
Axl	3.50	4.91						
RANTES	2.55	3.62						
TACI	2.47	9.46						
IGFBP-2	2.15	2.25						
M-CSF	2.06	8.09						

Each number indicates the ratio of normalized net fluorescent intensity of CPCs to BMs, AMCs, and SMs. The cytokines showing the ratio of normalized net fluorescent intensity more than 2.0 were presented. The results of 2 different samples were shown. AMC indicates adipose tissue-derived mesenchymal cell; BM, bone marrow mononuclear cell; CPC indicates cardiac progenitor cell; GCSF, granulocyte-colony stimulating factor; GITR, glucocorticoid-induced tumor necrosis factor receptor family-related gene; IGFBP-2, insulin-like growth factor binding protein 2; JAM-A, junctional adhesion molecule-A; MCP-1, monocyte chemotactic protein-1; M-CSF, macrophage colony-stimulating factor; MFG-E8, milk fat globule–EGF factor 8 protein; RANTES, regulated upon activation normal T cell expressed and secreted; SMs, skeletal myoblasts; sTNF RI, soluble tumor necrosis factor receptor I; TACI, transmembrane activator and calcium modulator and cyclophilin ligand interactor; TIMP1, tissue inhibitor of matrix metalloproteinase 1; TWEAK R, TNF-related weak inducer of apoptosis receptor; VCAM-1, vascular cell adhesion molecule 1; VEGF, vascular endothelial growth factor.

1% collagenase type 2 (Worthigton), 4.6 U/mL Dispase II (Life Technologies), and 2.4 mmol/L $CaCl_2$. After the enzymatic reaction was stopped by adding 5 mL of cold PBS with 3% FBS, the cells were suspended in cold PBS with 3% FBS and then filtered through a 70-μm cell strainer. Cells were stained at 4°C for 30 minutes simultaneously with 2 colors using the following antibodies: fluorescein PE-Cy5–labeled rat anti-mouse CD45, FITC-labeled rat anti-mouse Ly-6G, and control rat IgG2b. All antibodies were purchased from eBioscience. Cell fluorescence was measured with EPICS ALTRA flow cytometer using EXPO32 software, version 1.2 (Beckman Coulter, Inc). Heart cell isolation and flow cytometry were performed on 3 mice per PM-, CPC+PM–, or JAM-A+PM–treated group.

Detection of Proliferative Endogenous CPCs and Cardiomyocytes

To label the proliferating cells, 50 mg/kg BrdU (Sigma-Aldrich) was intraperitoneally injected into the mouse shortly after creating MI. The mice were treated with PM or JAM-A+PM. Administration of BrdU was continued every 12 hours for 9 days. After 2 weeks, the hearts were excised, and paraformaldehyde-fixed frozen sections were subjected to immunohistochemical analysis as described here earlier. For BrdU detection, 12% HCl was applied for 10 minutes before anti-BrdU antibody (eBiosciences) was applied. For Nkx2.5 (Abcam) detection, Tyramide Signal Amplification Kits (Molecular Probe) were used according the manufacturer's instruction. The images were obtained with laser confocal microscopy (TCS-SP5 Ver2.0; Leica Microsystems).

Statistical Analysis

The normality and variance of data were analyzed adjusted with a P value of 0.05 as the rejection criterion. Results are presented as mean±SEM. Statistical significance was calculated by using the unpaired Student t test for comparison between 2 groups or by 1-way ANOVA–Tukey–Kramer post hoc test for multiple comparisons. To assess expression-level changes in CD31 and JAM-A over time, 2-factor factorial ANOVA was used. In cases where the data were not normally distributed and/or the variances were not homogeneous, the

Table 3. Total Dataset of Net Intensity Ratio of Mouse Cytokine Array

CPCs vs BMs		CPCs vs BMs	
Description	Net Intensity (Ratio)	Description	Net Intensity (Ratio)
Decorin	243.6053593	Decorin	289.9391128
MFG-E8	27.83344467	MCP-1	32.01844262
Growth arrest specific 1	20.55963322	TWEAK R	24.60629921
MCP-1	18.98397752	Growth arrest specific 1	16.68112364
ACE/CD143	14.92782397	MFG-E8	13.56520795
VEGF	13.87443635	TIMP-1	11.63453596
JAM-A	10.98973559	VEGF	11.43053095
Pentraxin 3	10.79074586	VCAM-1	9.132837116
CD27	10.04580889	JAM-A	6.618177486
TIMP-1	9.956688405	Galectin-1	6.091580826
VCAM-1	9.644875678	GITR ligand	5.588652799
CD36	9.487486006	GCSF	4.944326879
TACI	9.458321905	sTNF RI	3.870478314
RAGE	8.942304253	Axl	3.504762973
GITR ligand	8.923870461	RANTES	2.551918788
TWEAK R	8.254911672	TACI	2.465841925
M-CSF	8.089109632	IGFBP-2	2.150204699
Prolactin	7.795143626	M-CSF	2.061830163
CD40 ligand	6.167091168		
IL-17F	5.970149254		
EGF	5.686212073		
Cardiotrophin-1	5.644615037		
IL-20	5.562199294		
E-cadherin	5.515689378		
sTNF RI	5.085538762		
Axl	4.914922688		
IGFBP-6	4.842310169		
Epiregulin	4.580852038		
Neprilysin	4.348620183		
IL-17B	4.34436948		
Amphiregulin	4.212441868		
Galectin-1	4.202969818		
Granzyme B	3.777176787		
RANTES	3.61856032		
IL-17E	3.389876473		
DKK-1	3.306167656		
HGF	3.228295363		
CXCL16	3.208676261		

Continued

Table 3. Continued

CPCs vs BMs		CPCs vs BMs	
Description	Net Intensity (Ratio)	Description	Net Intensity (Ratio)
IL-1R4/ST2L	3.172357347		
IL-21	3.132733937		
IL-28	3.116993224		
VEGF R1	2.977360153		
Endoglin	2.888804151		
MAdCAM-1	2.745585784		
4-1BB	2.589278316		
GCSF	2.585622902		
HAI-1	2.500606397		
MIP-3α	2.461647531		
IL-11	2.437425202		
IGFBP-2	2.24696379		
Epigen	2.129707719		
CPCs vs AMCs		CPCs vs AMCs	
Description	Net Intensity (Ratio)	Description	Net Intensity (Ratio)
VCAM-1	53.72011818	GCSF	7.488729462
MIP-1γ	31.50797152	JAM-A	3.012311316
Growth arrest specific 1	23.48354977	VCAM-1	2.479888107
MFG-E8	20.97623393		
JAM-A	20.63855695		
sTNF RI	16.48886177		
MCP1	15.4038109		
IL-1ra/IL-1F3	13.60100103		
ACE/CD143	12.95588521		
sTNF RII	10.13880017		
CD36	10.1361282		
RAGE	9.864462288		
Decorin	9.685230024		
TACI	9.212514279		
CD27	8.337224038		
Galectin-1	7.900391859		
IL-6 R	7.464636286		
RANTES	7.417572229		
GITR ligand	7.180967564		
CD40 ligand	7.065490027		
EGF	7.050843633		
Prolactin	6.247813265		
E-cadherin	6.179018525		
IL-17F	5.921714929		

Continued

Table 3. Continued

CPCs vs AMCs		CPCs vs AMCs	
Description	Net Intensity (Ratio)	Description	Net Intensity (Ratio)
IL-20	5.60950025		
M-CSF	5.414243793		
Amphiregulin	5.270897792		
CXCL16	5.184086927		
Granzyme B	5.071045345		
Pentraxin 3	5.070505377		
Epiregulin	4.833533119		
Neprilysin	4.570634587		
IGFBP-6	4.431956177		
VEGF	4.394773735		
HGF	4.286271501		
Axl	4.18075931		
Cardiotrophin-1	4.141815772		
4-1BB	3.949291102		
IL-21	3.563207742		
IL-28	3.32499867		
VEGF R1	3.242331885		
TWEAK R	3.223508402		
IL-17B	3.208120394		
MAdCAM-1	3.103286691		
MIP-3α	2.828550255		
DKK-1	2.756529529		
HAI-1	2.685493768		
Osteopontin	2.617437895		
GCSF	2.610679769		
Pro-MMP-9	2.448897629		
Endoglin	2.430818894		
IL-11	2.400147849		
Epigen	2.191636714		
IL-17E	2.168468302		
CPCs vs SMs		CPCs vs SMs	
Description	Net Intensity (Ratio)	Description	Net Intensity (Ratio)
JAM-A	25.03567584	JAM-A	16.05961328
ACE/CD143	5.537006584	VCAM-1	10.36924896
TACI	4.99797582	Pentraxin 3	8.343484573
RAGE	4.813246053	GCSF	5.857819017
Endoglin	4.256206613	GITR Ligand	3.964431124
EGF	3.917390078	Growth arrest specific 1	2.759427584

Continued

Table 3. Continued

CPCs vs SMs		CPCs vs SMs	
Description	Net Intensity (Ratio)	Description	Net Intensity (Ratio)
Epiregulin	3.789572612	Axl	2.324024839
GITR ligand	3.788553265	sTNF RII	2.221955588
Prolactin	3.669563175	IL-6 R	2.006175007
Cardiotrophin-1	3.573892004		
IL-17F	3.565214911		
IL-20	3.46275975		
VCAM-1	3.402772579		
HAI-1	3.358104954		
GCSF	3.357811781		
4-1BB	3.324335465		
Granzyme B	3.309526804		
CD36	3.282045896		
E-cadherin	3.237545164		
IL-1ra/IL-1F3	3.171703332		
IL-6R	3.060780989		
Neprilysin	3.05722514		
Pentraxin 3	3.038839406		
CD27	3.02893542		
CD40 ligand	3.004311187		
DKK-1	2.978885658		
Amphiregulin	2.925139822		
IL-17B	2.848207623		
MIP-3α	2.716623563		
IL-17E	2.588226159		
TWEAK	2.344572432		
IL-28	2.235206287		
IL-21	2.211239732		
MAdCAM-1	2.194450235		
IL-11	2.159332853		
IL-1R4/ST2L	2.040633086		
Epigen	2.003514164		

ACE indicates angiotensin converting enzyme; BM, bone marrow mononuclear cell; CPC; cardiac progenitor cell; DKK-1, Dickkopf-related protein 1; EGF, epidermal growth factor; GCSF, granulocyte-colony stimulating factor; GITR, glucocorticoid-induced tumor necrosis factor receptor family-related gene; HAI-1, hepatocyte growth factor activator inhibitor type1; HGF, hepatocyte growth factor; IGFBP-2, insulin-like growth factor binding protein 2; IL, interleukin; MCP-1, monocyte chemotactic protein-1; M-CSF, macrophage colony-stimulating factor; MFG-E8, milk fat globule–EGF factor 8 protein; MIP, Macrophage inflammatory protein; RAGE, receptor for advanced glycation end products; RANTES, regulated upon activation normal T cell expressed and secreted; sTNF RI, soluble tumor *necrosis factor receptor I*; TACI, *transmembrane activator and calcium modulator and* cyclophilin ligand interactor; TIMP1, tissue inhibitor of matrix metalloproteinase 1; TWEAK R, TNF-related weak inducer of apoptosis receptor; VCAM-1, vascular cell adhesion molecule 1; VEGF, vascular endothelial growth factor. The results of two different samples were shown.